The interplay between light, arsenic and H_2O_2 controls oxygenic photosynthesis in a Precambrian analog cyanobacterial mat.

Short title: Light, arsenic, and H_2O_2 govern photosynthesis in a microbial mat

Andrea Castillejos Sepúlveda[1,*], Daan R. Speth[2,3§], Carolin Kerl[4], Daniel Doherty-Weason[5,6,7], Federico A. Vignale[8], Kinga Santha[1], Wiebke Mohr[2], Arjun Chennu[9], Elisa Merz[1], Dirk de Beer[1], Maria E. Farias[10], Judith M. Klatt[1,5,6,7*].

[1] Microsensor Group, Max Planck Institute for Marine Microbiology, Bremen, Germany.

[2] Biogeochemistry Group, Max Planck Institute for Marine Microbiology, Bremen, Germany.

[3] Division of Microbial Ecology, Centre for Microbiology and Environmental Systems Science, University of Vienna, Vienna, Austria.

[4] Environmental Geochemistry, Bayreuth Center for Ecology and Environmental Research (BayCEER), University of Bayreuth, D-95440 Bayreuth, Germany

[5] Microcosm Earth Center, University of Marburg & Max Planck Institute for Terrestrial Microbiology, 35032 Marburg, Germany

[6] Center for Synthetic Microbiology (SYNMIKRO), Karl-von-Frisch-Straße 10, 35032 Marburg, Germany

[7] Biogeochemistry Group, Department of Chemistry, University of Marburg

[8] European Molecular Biology Laboratory - Hamburg Unit, Notkestrasse 85, Hamburg 22607, Germany

[9] Leibniz Centre for Tropical Marine Research, Data Science and Technology, Fahrenheitstr. 6, 28359 Bremen, Germany

[10] PUNABIO S.A. Campus USP-T Av. Solano Vera y Camino a Villa Nougués, San Pablo, Tucumán, Argentina

*Correspondence: andreacasbio@gmail.com, Judith.Klatt@mpi-marburg.mpg.de

Abstract

The regulation of O_2 production by cyanobacteria is critical to understanding the co-evolution of oxygenic photosynthesis (OP) and Earth's redox landscape. This includes their response to electron donors for competitive anoxygenic photosynthesis, like arsenic. In this work, we assessed the effect of arsenic cycling on photosynthetic activity in a modern cyanobacterial mat thriving beneath an arsenate-rich (~9-10 µM) water column in the high-altitude central Andes, using biogeochemical and omics approaches. Microsensor measurements and hyperspectral imaging revealed two O_2-producing cyanobacterial layers. During the afternoon, OP ceased in the lower, Chl *f*-dominated layer. Ex-situ measurements revealed that the combination of high light and arsenic induced a prominent rise in local H_2O_2 concentration, which then coincided with the interruption of OP. Mat incubations suggested that after OP ceased, cyanobacteria transitioned to As(III)-driven anoxygenic photosynthesis using far-red light. Additional incubations and metatranscriptomics on in-situ samples reveal simultaneous As(V) reduction during the day, at sufficiently high rates to supply electron donors for anoxygenic photosynthesis. This study proposes that As(III) can serve as an alternative electron donor for cyanobacterial photosynthesis. It also reveals the crucial role of arsenic in moderating OP, a consequence of the interaction between arsenic and reactive oxygen species under high irradiance. Given the widespread abundance of arsenic in the Precambrian, we further discuss how this regulatory mechanism could have played an important role in the early evolution of OP.

keywords

ROS arsenic cyanobacteria redox GOE anoxygenic photosynthesis

1. Introduction

Oxygenic photosynthesis (OP) evolved in cyanobacteria during the Archean, a period referring to 3.7 to 2.5 billion years ago, within the Precambrian eon. The general consensus is that the evolution of OP was preceded by anoxygenic photosynthesis (AP) [1], in which reduced substances (e.g. sulfide, ferrous iron, arsenite) were used as electron donors for light-driven carbon fixation. These electron donors were widely available in the mostly reducing environment of the Archean oceans [2]. Intriguingly, extreme volcanic activity resulted in high arsenic concentrations, i.e. high reduced inorganic arsenite (As(III)) [3,4]. Given its prevalence, As(III) could have been a widespread electron donor for AP during the Archean [5], and may have sustained an active redox cycle, given that bacteria can metabolize both arsenate (As(V))) or As(III) for energetic gain [6].

It is widely accepted that ancient cyanobacteria, seeking protection from both the intense UV radiation and resulting reactive oxygen species (ROS), avoided surface layers with direct strong irradiation. Cyanobacteria could have instead positioned themselves under mineral crusts or, or deeper inside stratified microbial communities, known as microbial mats [7]. This represents a fragile compromise between harvesting photosynthetic light and preventing exposure to UV radiation. Consequently, early cyanobacteria might have developed diverse strategies to harness low-energy light and exploit a diverse set of spectral niches. One intriguing strategy is known as FaR-Red Light Adaptations [8–10], which involves the utilization of chlorophyll f (Chl *f*) to harvest light at approximately 710 nm. The use of Chl *f* could potentially signify an ancient trait developed by cyanobacteria[11].

In addition to optimizing light harvesting, modern cyanobacteria exhibit metabolic flexibility, enabling them to navigate complex environments. Certain strains demonstrate the remarkable capability of engaging in both OP and sulfide-driven AP [12–14]. Interestingly, light capture and type of photosynthesis might be linked through small differences in D1, a core protein of PSII, which is essential for OP. Chl *f* synthesis requires the exchange of D1 (in photosystem II), for a similar protein (super-rogue D1) that functions as a Chl *f* synthase [15]. As a result, OP is blocked, possibly favoring

70 PSI-based AP through the far-red light capture via Chl *f* [15,16]. To date, only sulfide has been
71 confirmed as an electron donor for cyanobacterial AP, with well-documented and highly species-
72 dependent responses to sulfide exposure [17,18]. Although sulfur and arsenic metabolism seem
73 evolutionarily interconnected [19], our understanding of how cyanobacteria manage arsenic
74 exposure remains limited.

75 Studying modern analogues of Precambrian environments, such as the isolated lakes and wetlands
76 in the central Andes with their extreme conditions, offers valuable insights into potential interactions
77 between OP and arsenic cycling on ancient Earth [20–24]. Among those ecosystems, Laguna Pozo
78 Bravo, located in the Salar de Antofalla, Argentina, represents an ideal study site as environmental
79 pressures there include high altitude, intense UV radiation, drastic shifts in air temperature, and high
80 arsenic concentrations due to the volcanic origin of the Andean mountain chain [25,26]. Laguna Pozo
81 Bravo harbors thriving microbialites and microbial mats despite the seemingly harsh environmental
82 conditions [25,27]. Similar microbial mats and microbialites were abundant in submerged
83 environments through the Precambrian [28].

84 In microbial mats, functional groups of microorganisms form distinct vertically-stratified layers
85 according to their metabolic niches. Due to the close proximity of different microorganisms,
86 metabolites diffusing across layers of the mat can be efficiently recycled. However, bacteria in mats
87 also encounter challenges from competition for resources, as well as the quick spread of hazardous
88 metabolites, such as sulfide, arsenic and ROS, from neighboring layers.

89 In this study, we combined incubation experiments with microsensor- and omics- based approaches
90 to assess the interactions between arsenic and diel dynamics of OP. We hypothesized that OP is
91 fundamentally influenced by local arsenic speciation, which is shaped by the co-inhabiting
92 microorganisms, and that the regulation is predominantly mediated via ROS and competition with
93 AP.

2. Results

2.1. Description of Laguna Pozo Bravo and their microbial mats

Laguna Pozo Bravo is a hypersaline lake at an altitude of 3330 m [25]. During our sampling in February 2019, the water column had a pH of ~8.00 and high salinity (137.25 g L^{-1}). Irradiance reached extremely high levels at noon (up to 2950 µmol photons m^{-2} s^{-1}). Air temperature fluctuated greatly through the day (4°C at night, 30°C at noon), while water temperature remained around 20°C.

The lake sediment was mostly covered by light pink microbial mats, interspersed with patches of dark gray lithifying mat zones and microbialites (Fig 1a; Lencina et al., 2021). The microbial mats displayed a vertical stratification into four distinct visible layers: a pink upper crust rich in calcium carbonate, a green layer, a red layer, and a brown layer (Fig 1b). The mats form cohesive sheets and can be easily separated from the underlying coarse dark brown sediment. Hyperspectral imaging showed that the green layer consisted of a zone dominated by Chl *a* (absorption max at 690 nm) and phycocyanin (absorption max at 625 nm) indicative of cyanobacteria [29,30], and a zone dominated by BChl *a* (absorption max at 810 nm [31]) indicative of purple anoxygenic phototrophs [32] (Fig 1d). The red layer showed a clear absorption maximum at 715 nm, characteristic of specific BChl e in green anoxygenic bacteria like Chloroflexi [33] or of Chl *f* in cyanobacteria [34]. No spectral signs of photosynthetic pigments were found in the pink and brown layers.

Fig 1. Overview of microbialites and microbial mat structures in Pozo Bravo. (a) Microbialites and microbial mats (pink and lithifying gray) found in Pozo Bravo, (b) Pink microbial mat cross section, with layers indicated. (c,d) Distribution of selected pigments in the top 7 mm of Pozo Bravo microbial mat, captured by hyperspectral imaging. c) Regular view, see Supp. Fig S1 for a different view of the same sample, with brighter color banding. The microbial mat surface is indicated by a white line. (d) Second derivative of reflectance spectra around 675 nm, 715 nm, and 805 nm as indicated by different colors. Pigments with in-vivo absorption maxima at the respective wavelength are shown in parentheses.

2.1.1. Microbial mat metagenome analysis

To investigate the vertical distribution of phyla in the mat, we performed metagenomics on slices of a microbial mat. The slices were obtained by separating a piece of mat with a scalpel into the four visible layers (pink, green, red, brown, Fig 1b), directly after sampling. An assembly was then made using the metagenomic reads from all layers. After assigning the assembled contigs to bins, between 62-69% of the reads from each layer were successfully mapped back to the bins, indicating that the bins give a good overview of the microbial community in each layer (Fig 2, Supp. Table S2). Among bins with taxonomic assignments, Pseudomonadota (Alphaproteobacteria and Gammaproteobacteria) was found to be the most abundant phylum across all layers of the microbial mat, followed by Bacteroidota (Bacteroidia and Rhodothermia) and Bacillota (Halanaerobiia, Bacilli, and Clostridia). Chloroflexota (Chloroflexia and Anaerolineae) were also abundant in all layers except for the upper crust, while Deinococcota (Deinococci) were present in a relatively large abundance only in the crust. With the exception of an incomplete Lokiarchaea bin in the red and brown layers, all bins were bacterial. Two cyanobacterial bins, *Halothece sp*. and ESFC-1 (of family *Spirulinaceae*), were recovered from a co-assembly made using all samples. A new assembly was conducted only using reads from the green microbial mat layer to specifically target cyanobacteria. The same cyanobacterial bins, plus RECH01 (of family *Elainellaceae*), were recovered. From the abundance of reads mapped to each bin (Supp. Table S3), ESFC-1 and RECH01 were likely located in the pink and green layers, and Halothece in the green and red layers.

Although pigment absorbance (Fig 1d) indicated a relatively high abundance of cyanobacteria in the green and red layers of the microbial mat, total cyanobacterial abundance in the mat appears to be underestimated. For possible reasons behind this discrepancy see Supplement to Results 2.2. The relative abundance between the cyanobacterial taxa per mat layer, however, likely reflects the real vertical distribution under the assumption that DNA extraction efficiency is similar for all cyanobacteria through the mat.

Fig 2. Taxonomic profile of phyla from metagenomic bins in a Pozo Bravo microbial mat. The bins were selected from a metagenomic assembly made using reads from all vertically-stratified layers (crust, green, red, brown). Only bins with over 55% completeness and less than 10% redundancy are shown. Relative abundance was obtained by mapping the reads from each individual layer metagenome to the total set of bins. Results were summarised by grouping bins by phylum.

2.1.2. Arsenic redox pathways in the metagenome

We then used our metagenome data to screen for genes involved in arsenic metabolism. A great variety of genes directly related to arsenic metabolism are present in the Pozo Bravo microbial mat, to the abundance of housekeeping genes(Fig 3). The roles of these genes are discussed in more detail below and shown in Fig 2b, Supp. Results 2.3, and Supp. Table S1.

Several distinct routes for microbial arsenic detoxification exist, broadly divided into three steps. Initially, arsenic gets imported into microbial cells via specific transporters, then it is chemically modified by specific detoxification systems, and then finally exported using dedicated efflux systems. First, we focused on arsenic import pathways. As(V) and As(III) can enter the cell through different mechanisms. As(III) (in the protonated form $As(OH)_3$) can enter the cell by diffusion across the membrane or through aquaglyceroporin channels (*aqps*), the genes for which were found in the metagenome [35,36]. As(V) can be imported through phosphate channels [37]. Almost all components (*pstSCAB*) of the high-affinity phosphate import channel were found. The pst system is also highly selective for phosphate because the slightly larger size of As(V) affects crucial bonds in the transporter, thus allowig the discrimination of phosphate over arsenate by 500- to 4500-fold [38]. Thus, the use of pst indicates an adaptation to limit As(V) intake (see Supp. Results 2.3) [37–39].

Once inside the cell, arsenic can be metabolized for energy generation or detoxified through a series of redox reactions. The genes found in the Pozo Bravo metagenome were summarized into three putative detoxification-related pathways (Fig 3): The first detoxification pathway is based on an As(V)-transferring gap3/gadph, and arsJ, which were both found in the metagenome. The second pathway involves reduction of As(V) to As(III) via arsC1, arsC2 and mrx1. The genes encoding for arsC1 and arsC2 were? not recovered from the metagenome. Yet, their presence is required for

functionality of mrx1 (Fig 3, for the full Mrx1 cycle see Ordóñez et al. 2009 [40]. While this pathway has thus far exclusively been assigned a detoxification function, the third pathway involving As(V) reduction mediated by the product of the genes *arsRCDAB* and *acr3*, has been hypothesized to be used in As(V) respiration [41]. In all other studies of genomes and metagenomes in the Puna region, an environment similar to Pozo Bravo, *acr3* was the predominant As(V) reduction gene [23,42,43]. No other respiratory *arrA* or *arrB* As(V) reductases were found. As(III) oxidation is mediated by the products of *aioA* and *aioB*, coupled to the reduction of either cytochrome c or azurin, as part of processes such as AP [44]. Both *aioA* and *aioB* were found in reads from all layers of the metagenome. Other arsenite oxidation genes (*arxA*) were not found in the metagenome. Overall, the metagenomic analysis revealed a significant abundance of arsenic-related genes in all layers of the Pozo Bravo microbial mat, thus enabling bacteria to thrive under these harsh conditions.

Fig 3. **Pathways of arsenic metabolism present ain Pozo Bravo microbial mats.** (a) Presence of genes associated with arsenic cycling and housekeeping genes (DNA gyrase (*gyrA*, *gyrB*)) in the metagenome of Pozo Bravo microbial mat. Shades of gray represent the number of gene copies (normalized as Transcripts Per Million, TPM [45]) from each microbial mat layer that were mapped to the metagenomic assembly, which was made using reads from all microbial mat layers. Almost as many gene copies are dedicated to arsenic cycling as for housekeeping tasks, suggesting intense metabolizing of arsenic species. (b) Overview on the pathways of redox arsenic transformation detected in Pozo Bravo mats, based on previously reported functions of arsenic genes [6,40,46,47]. Genes were broadly classified in expressing transporters for arsenic uptake (blue) and export (red), enzymes involved in reduction of As(V) (orange), oxidation of As(III) (green), and production and export of organic arsenicals (pink). ArsC1 and ArsC2 are shown in gray since their presence could not be determined in the metagenome). Details and a list of abbreviations can be found in Table S1.

2.2. In-situ dynamics of oxygenic photosynthesis and dissolved arsenic speciation

To assess the dynamics of photosynthetic O_2 production under the hostile and dynamic conditions of Pozo Bravo, we performed in-situ microsensor depth profiling. This revealed that OP occurred in two distinct layers within the mat. An upper O_2 concentration peak was observed at approximately 1 mm depth (Fig 4a & d, Supp. Fig S2) in the green Chl *a*-dominated layer (Fig 1d). An additional net OP

maximum was observed at approximately 2-3 mm depth (Fig 4a & d, Supp. Figs. S3-S4), coinciding with the depth of the red microbial mat layer. The production of O_2 in this layer strongly suggests that the dominant pigment with the absorption maximum of 715 nm is cyanobacterial and hence Chl *f*, instead of BChl e.

The rates of net OP in both layers exhibited unusual dynamics over a diel cycle. In the top cyanobacterial layer, net OP decreased at high light intensities after noon but recovered again in the late afternoon (Fig 4a & d, Supp. Figs S3-S4). This pattern was more pronounced in the deeper Chl *f*-cyanobacterial layer, where OP was completely interrupted at around 13:00 and only resumed around 18:00 in one of the two replicate spots (Fig 4a, Supp. Fig S2).

To assess co-occurring changes in the concentration of electron donors for AP, H_2S dynamics were measured using microsensors, and the speciation dynamics of iron and arsenic were determined through porewater analysis. The insubstantial dynamics of both iron and H_2S suggests that neither drive AP (see Suppl. Results, Supp. Figs. S5). However, arsenic speciation in the porewater underwent strong changes over the diel cycle. Although the depth resolution obtained was low, porewater measurements clearly showed the greatest changes in redox cycling of dissolved arsenic within the top centimeter of the microbial mat, i.e. in the photic zone (Fig 4b & c). Here, up to 98% of dissolved arsenic was oxidized during daylight hours (07:00-18:00), and reduced at 19:00 and in the predawn hours (00:30-06:00) (Supp. Fig S6). Measurements could not be obtained between approximately 19:00 – 00:30 due to strong winds, but we assume that dissolved arsenic were reduced during this time period. Thus, the interruption of OP in the deep cyanobacterial layer coincided with a maximum in As(V) and minimum in As(III) concentration.

Fig 4. Interruption of cyanobacterial photosynthesis coincides with strong redox dynamics in dissolved arsenic. Depth profiles of dissolved oxygen (a), and speciation of inorganic arsenic over a diel cycle in porewater from Pozo Bravo (b&c, n=1-3 per depth). The microbial mat surface is at 0 cm depth (horizontal white line in (a-c), black dotted line in (d)). Profiles selected from various points in time are shown in (d). The timepoints used for d) are indicated by rectangles in (a-c), following the numbering in (b). Profile 4 represents a single point in time (00:30). Colored background represents the estimated placement of the green and red microbial mat layers (Fig 1b). The chosen profiles exemplify the oxygen production during the morning (d1) and late afternoon (d3), with a period of interruption in between (d2). D4)shows a comparison of the dissolved arsenic speciation at night (00:30). The interruption in oxygen production coincides with a maximum in dissolved As(V). Net volumetric rates calculated based on the concentration depth profiles of oxygen measured in two replicate spots can be found in Supp. Fig S3, and depth integrated rates over a diel cycle in Supp. Fig S4.

2.3. A combined effect of light and arsenic on H_2O_2 and oxygenic photosynthesis

To test if the interruption of OP at noon was related to arsenic or exclusively to light, depth profiles of O_2 were measured ex-situ in microbial mats before and after As(V) addition at increasing light intensities, from low to high light (~500 to ~1000 µmol photons s^{-1} m^{-2}) (Supp. Fig S7). Arsenic was added the evening prior to the measurements to allow for diffusion into the mat and reestablishment of internal redox cycling. The results revealed a combined effect of both arsenic and light intensity on OP. In the microbial mat without arsenic, local O_2 concentration increased until reaching a steady state under both high and low light conditions, as expected from normal cyanobacterial OP. However, O_2 production ceased after approximately 30 min in microbial mats treated with As(V) (to 10 µM final concentration) when exposed to high light. O_2 production resumed after lowering light intensity, showing that OP was hindered only in the presence of both arsenic and high light. Although most mat pieces did not exhibit the clearly separated double peaks observed in-situ, occasionally two net productivity maxima were observed. The inhibitory effect of light and arsenic occurred more rapidly and extensively in the deeper maximum. OP was also interrupted in As(V)-supplemented mats that were instantly exposed to high light and not to a stepwise increase. Thus, the interruption of OP appeared to be independent of exposure time to light and time of day, and exclusively driven by a combined effect of high light and arsenic.

To further elucidate the mechanism behind the inhibition of OP, we simultaneously measured H_2O_2 concentration in depth profiles (Fig 5). In the absence of arsenic, no net production of H_2O_2 was observed across light intensities. In As(V)-treated mats, H_2O_2 concentration within the photosynthetically active zone dramatically increased at 1000 µmol photons m^{-2} s^{-1}. Upon the cessation of OP, H_2O_2 concentrations decreased to values comparable to dark conditions. Notably, a transient increase of H_2O_2 at the oxic interface was observed in live mats treated with both arsenic and DCMU, an inhibitor of OP (Fig 5f). Although the increase in H_2O_2 was much smaller when OP was inhibited, the increase was nevertheless surprising as OP was expected to be the only source of H_2O_2. Moreover, measurements following the addition of approximately 200 µM H_2O_2 to the water column, demonstrated that OP remained unaffected and H_2O_2 was entirely consumed within the first 1-2 mm (Supp. Fig S8), as also observed in other mat systems [48]. In summary, these results suggest three key findings: (1) H_2O_2 production is related to a light-driven mechanism in the presence of dissolved arsenic. Due to the possibility of arsenic cycling within the mat, the arsenic species triggering ROS production and OP interruption remains unclear. (2) The resultant local H_2O_2 production rate must be enormous, overwhelming the substantial sink strength. (3) Given that H_2O_2 production occurs in the presence of DCMU (01:00 in Fig 5f), but not in the phase of OP discontinuation (15:00-17:00 in Fig 5f), the mat community likely transitions to an activity that tempers ROS abundance when no OP occurs.

Fig 5. As(V) inhibits OP at high light and induces H_2O_2 evolution. O_2 and H_2O_2 measurements of microbial mats before (a-c) and after As(V) addition (10 µM final concentration) (d-f)). Bars over each graph represent light conditions over time, as either darkness, low light (500 µmol photons m^{-2} s^{-1}), or high light (1000 µmol photons m^{-2} s^{-1}). Contour plots show concentration of O_2 (a,d) or H_2O_2 (c,e) across the depth of the microbial mat over time. The solid white horizontal line represents the mat surface at depth 0. The vertical dashed line in d-f indicates time of DCMU addition, an inhibitor of oxygenic photosynthesis. (c) and (f) Depth-integrated rates of production (DIR) for O_2 (n=3 pieces of mat) and H_2O_2 (n=2 pieces of mat).

2.4. Transition from oxygenic photosynthesis to light-driven As(III) oxidation in cyanobacteria using far-red light

To assess the interaction between dissolved arsenic speciation and photosynthesis, microbial mat pieces were incubated, with and without an OP inhibitor (DCMU), over a diel cycle using various light qualities targeting different phototrophs. This showed that As(V) reduction occurred under most treatments in the dark (Fig 6, Supp. Figs. S9-S12). Second, we found AP under all light conditions, including those specifically targeting cyanobacteria (Fig 6).

Incubations were initiated by the addition of As(V) or As(III) to enable differentiation between oxidation and reduction rates. Total dissolved arsenic remained relatively constant in all incubations, suggesting that sorption/desorption dynamics played a minor role. This also allowed us to calculate rates of both As(III) oxidation and As(V) reduction based only on As(V) dynamics, which was favorable due to the higher accuracy of the employed colorimetric method for As(V) [49]. The incubations showed a strong dependence of arsenic speciation on light (Fig 6, Supp. Figs. S9-S12). Most notably, As(V) was consistently reduced in the dark, indicating respiration with As(V) as the electron acceptor. Upon exposure to all types of light, rates of reduction consistently dropped (Supp. Figs. S9-S12). Full spectrum white light and 715 nm light even triggered net As(V) production, i.e. net As(III) oxidation, albeit with a delay under 715 nm light (Fig 6a & e, Supp. Figs. S9 & S10).

Given that As(V) respiration and photosynthetic As(III) oxidation likely co-occur, we conducted a detailed analysis of As(V) consumption (i.e., respiration) rates to estimate photosynthetic gross rates from net rates. Rates of As(V) consumption in the dark were linearly dependent on As(V) concentration across the complete measured range (Fig 4b). Assuming that As(V) respiration rates were unaffected by light and solely determined by the As(V) concentration, we were able to calculate light-driven gross As(III) oxidation as

$$G\_As(III)_{oxidation} = N\_As(V)_{prod} + As(V)_{resp}([As(V)]) \quad (1)$$

where $G\_As(III)_{ox}$ is the gross rate of As(III) oxidation (i.e. gross As(V) production, Fig 6b), $N\_As(V)_{prod}$ is the net rate of As(V) production, (i.e. net As(III) oxidation), and $As(V)_{resp}([As(V)])$ is the rate of light-

303 independent As(V) consumption as a function of concentration derived from the linear regression in
304 Fig 6d.

305 These considerations revealed light-driven gross As(III) oxidation under all light treatments. The rates
306 were highest in full-spectrum white light in the absence of DCMU, i.e. under highly oxic conditions
307 favoring aerobic oxidation of As(III) (Fig 6b). Rates under these white light conditions were
308 substantially lower in the presence of DCMU but not absent, suggesting that As(III) was also truly
309 photosynthetically oxidized in the absence of O_2 derived from OP. At 810 nm, purple bacteria
310 oxidized As(III) by anoxygenic photosynthesis as previously observed in various cultures [5,44] and in
311 mats [24]. Intriguingly, at 690 nm and at 715 nm, which specifically target cyanobacterial Chl *a* and *f*,
312 respectively, we also found evidence for As(III)-driven AP (Fig 6b). Most strikingly, gross As(III)
313 oxidation occurred in the presence of DCMU, strongly suggesting that As(III)-driven photosynthesis
314 indeed occurs in the cyanobacteria from Pozo Bravo.

315 The regulation of As(III)-driven photosynthesis differed between the 690 nm and 715 nm treatments.
316 In the 690 nm treatments without inhibitor, O_2 production was only triggered after As(III) depletion
317 indicating that the cyanobacteria transitioned from As(III)-driven anoxygenic photosynthesis to OP
318 upon depletion of the alternative electron donor (Supp. Fig S9, Fig 6c). For incubations under 715 nm,
319 the diel patterns in photosynthesis dynamics were similar to those observed in porewater extracted
320 from mats (Fig 6a,c,e, Supp. Fig S10): Net OP occurred within the first hours of light exposure (phase
321 1) and then ceased (phase 2) (Fig 6e). For treatments with and without DCMU, As(V) release was
322 absent in phase 1 (first hours of light exposure), but increased drastically in the afternoon (phase 2)
323 (Fig 6e). Due to the lack of oxygen in treatments with DCMU, the phases for this treatment were
324 estimated by the change in As(V) release partway through the experiment, rather than by net OP.
325 Only the 715 nm treatment exhibited these two clear phases. The similarity in gross As(V) production
326 with and without DCMU at 715 nm strongly suggests that As(III) is oxidized by cyanobacteria using
327 Chl *f* via anoxygenic photosynthesis after the interruption of OP.

Fig 6. Rates of arsenic cycling dependent on light quality and photosynthesis. (a) Net rates of As(V) production (Net_As(V)$_{prod}$) in incubations of mat slurries with and without DCMU, under white light, light at λmax = 690 nm to target Chl *a*, λmax = 715 nm to target Chl *f*, and light at λmax =810 nm to target BChl *a*. The gray bars overlaid in 715 nm represent phase 1 and phase 2 of As(V) production, as shown in (e). (b) Rate of As(V) consumption, i.e. As(V) respiration, in the dark dependent on the concentration of As(V). (c) Gross rates of As(III) oxidation (G_As(III)$_{oxidation}$) calculated from (a) by adding the expected rate of As(V) removal (As(V)$_{resp}$([As(V)]) from (b) according to Eq (1). (d) Net rates of oxygenic photosynthesis in the same incubations as in (a) and (c). In (e) an example for a time series of dissolved As(V) and O_2 in batch incubations is shown, based on which the net rates of arsenic production in (a) and net OP in (d) were calculated. The slurry was initially exposed to ~20 µM As(V) and, after a dark phase, exposed to light of λmax = 715 nm. Errors represent the standard deviation of concentration in separate vials (n=3). In phase 1, which represents the initial hours of exposure to light, net O_2 production occurred and arsenite was not photosynthetically oxidized. In phase 2, after sustained exposure to light, O_2 production ceased and As(III) was photosynthetically oxidized to As(V). A similar pattern was observed in the treatment with DCMU, which blocks OP. Namely, As(V) was reduced for an initial five hours (phase 1), after which As(III) was photosynthetically oxidized to As(V) (phase 2). Additional time series at different light qualities and with different initial arsenic conditions are in Supp. Figs. S9-S12.

2.5. Metatranscriptomic evidence for observed activity transitions

2.5.1. Concurrent arsenic oxidation and reduction

We used metatranscriptomes from Pozo Bravo to determine diel dynamics in transcription of genes related to arsenic metabolism. Specifically, we investigated photosynthetic gene transcription in the afternoon, and whether transcription of genes related to arsenite oxidation increased during the same period. For this purpose, we mapped transcriptomic reads from in-situ mat samples obtained over a diel cycle to the metagenomic bins (Fig 3a,7). This analysis generally supported our process rate observations of concomitant oxidation and reduction reactions and revealed mechanistic insights. Unfortunately arsenic cycling by cyanobacteria could not be assessed, except for *arsR*, and As(III) efflux encoders *arsA, arsB,* and *acr3;* and importers *pstSCAB* in the Halothece and ESFC-1 bins. The genes linked to arsenite oxidation in cyanobacteria may be currently undescribed, or highly divergent from sequences in databases. Also, few metatranscriptomic reads mapped to the cyanobacterial bins in general.

359 The highest read numbers mapped to arsenic genes were present in Alpha- and Gamma-
360 proteobacterial bins (Fig 7a), which stimulated in-depth analysis of diel transcription by these groups.
361 We found that As(III) oxidation was likely mainly driven by *aioAB* transcribed by taxa among the
362 Rhodobacterales and Chromatiales, prominent representatives of purple photosynthetic bacteria.
363 Specifically, *aioA* encoding for the large subunit of arsenite oxidase, was transcribed at all timepoints
364 in Rhodobacterales (Alphaproteobacteria) (Fig 7). The highest *aioA* transcription, and thus potentially
365 As(III) oxidation, happened during the day (9 am - 6 pm) although most of the arsenic present in
366 porewater was As(V) (Fig 7a). Transcription of *aioB*, which encodes for the small subunit of the same
367 As(III) oxidase, was also found during 9 am to 3 pm, in line with high *aioAB* activity during this portion
368 of the day. During daylight hours, Rhodobacterales expressing *aioAB* also transcribed *pufL* and *pufM*
369 (Supp. Fig S14), which encode for components of a type II photosynthetic reaction center, thus
370 supporting arsenite-driven anoxygenic photosynthesis. Similar patterns of *aioAB* and *pufLM*
371 transcription were observed in Rhizobiales, mainly during the morning and late afternoon (Supp. Fig
372 S14, Fig 7b).

373 Gammaproteobacteria were separated into three main orders: Chromatiales, Pseudomonadales and
374 Xanthomonadales (Fig 7b). Transcription of *pufLM* was found in both Pseudomonadales and
375 Xanthomonadales during the day as well as the night. However, unlike in Alphaproteobacteria,
376 transcription of *aioA* primarily took place during the night, except for Chromatiales that showed
377 transcription at 3 pm. Transcription of *aioB* was not found. This could suggest non-photosynthetic
378 As(III) oxidation at night, i.e.- coupled to nitrate reduction [50,51], in analogy to
379 chemolithoautotrophic sulfide oxidation by purple sulfur bacteria commonly observed in other mat
380 ecosystems [52].

381 The potential As(III)-oxidizing purple anoxygenic phototrophs among the Alphaproteobacteria
382 appeared to transition to As(V) reduction at low light and in the night. Namely, in Rhodobacterales,
383 the transcription of 1-arseno-3-phosphoglycerate via As(V)-transferring GAPDH and *arsJ* peaked at
384 night, and As(V) reduction and As(III) excretion via *arsC* and *arsB*, occurred in the morning. Most

Gammaproteobacteria did not show such pattern. Instead, *arsC*, *acr3* and *arsB* were continuously expressed. Chromatiales, however, co-expressed *aioA* and genes involved in excretion of intracellular As(III) (*arsA*, *arsB*) during the day. This general pattern of alternating key players in As(V) reduction held true across the complete metatranscriptome. Most prominently, the relative contribution of bacterial classes driving arsenate reduction via *arsC* changed per timepoint (Fig 7a). Transcription of *arsC* by Gammaproteobacteria was high and relatively constant, while *arsC* transcription at 9 am was highest by Alphaproteobacteria, and at noon by Bacteroidota and Chloroflexota. Spirochaetia was the only known bacterial class to express *arsC* at night (1 am), but some transcription was also found in unidentified bins. Transcription in unbinned reads was negligible. While the key players may alternate over a diel cycle, intriguingly, the general *arsC* transcription was highest during daylight hours (Fig 7a), consistent with pronounced cryptic redox cycling of arsenic.

Fig 7. Transcription of arsenic metabolism genes over a diel cycle in Pozo Bravo microbial mats. (a) Sum of *aioA*, *arsC*, and *grxC* transcription, in TPM, over the metatranscriptome of all layers of Pozo Bravo microbial mat. *aioA* is involved in arsenite oxidation, *arsC* is involved in arsenate reduction, and *grxC* may be part of arsenate reduction or reactive oxygen species response pathways. (b) Transcription of genes related to arsenic cycling in selected taxa, shown as the sum of TPM per gene, normalized across all timepoints (i.e., per column). Normalization was performed due to the varying number of gene copies found per gene. Higher gene transcription is represented in red, lower transcription in blue. Transcription of *pufL* and *pufM*, which encode for photosynthetic reaction center II, can be found in Supp. Fig S14. An overview of transcription of genes in cyanobacterial bins can be found in Supp. Fig S15.

2.5.2. Elevated general stress and ROS response prior to the interruption of OP

To confirm the involvement of ROS in the interruption of OP, we focused on the transcription of genes related to ROS response and stress. The transcription of genes involved in ROS repair peaked at 9:00 and 12:30 (Fig 7b), with few exceptions in the early morning and late afternoon (see Supp. Results 2.4). The transcription of ROS genes through the entire day may indicate that microbial mat inhabitants plausibly have to deal with continuous ROS stress, despite no net production.

Only a few reads from the metatranscriptome sample at 12:30 mapped to cyanobacterial genes, among which the stress proteins PspA and Hsp70 in RECH01 were of interest (Supp. Fig S15). *pspA* is a component of a phage shock protein involved in lipid membrane repair, while Hsp70 is a highly conserved heat shock protein found under both normal and stressful conditions in cyanobacteria. As suggested in previous reports [53,54], it is likely that in this case, *pspA* transcription is a response to membrane disturbance rather than an attack from phages. This is due to ROS production, from the intense light, potentially disrupting the membrane and highlighting the stress that cyanobacteria face at noon when OP is also interrupted.

2.5.3. Changes in cyanobacterial photosystems

Cyanobacterial bins showed clear differences in the gene transcription of the two photosystems over a diel cycle. Most prominently, the majority of PSI components were expressed in the morning, while those of PSII were expressed in the evening. The former could be consistent with the re-instatement of photosystems after a period of darkness. The latter suggests fundamental changes, like the repair or replacement of central photosystem components, when the cyanobacteria transition back to OP. Interestingly, the transcription of *psbA*, a central component of PSII, was highest shortly before the reinstatement of OP was observed (Supp. Fig S16). Diverse isoforms of D1, the protein encoded by *psbA*, are used by cyanobacteria based on changing environmental conditions, such as irradiance and O_2 concentration [55]. While it is known that D1 requires constant replacement due to ROS damage by the neighboring oxygen-evolving complex during OP, it is possible that AP also leads to radical formation in PSII when excitation energy cannot yield charge separation [56]. Thus, D1 replacement via *psbA* would enable cyanobacteria performing AP to replace D1 due to the accumulating ROS damage from AP, and/or express a different isoform of D1 better adapted to OP.

3. Discussion

As(III)-driven anoxygenic photosynthesis by bacteria has only been characterized in a small number of organisms, mostly in Mono Lake, an arsenic-containing environment [5,44,57]. In the cyanobacteria-dominated and arsenic-rich environment of Laguna Pozo Bravo, it appears to be the

438 dominant form of AP despite the low local concentration of As(III) in the mat. Omics and process
439 rates consistently suggest that AP was driven by a constant supply of As(III) from As(V) reduction in a
440 highly active, cryptic redox cycle of arsenic. The photosynthetic As(III) oxidation was performed by
441 various bacterial groups throughout the day. As expected, obligate anoxygenic phototrophs (purple
442 bacteria) utilized arsenic for photosynthesis (Fig 3&7). Surprisingly, As(III) appears to also be used by
443 cyanobacteria for AP. The regulation of the transition between OP and AP in the cyanobacteria is
444 complex, with ROS likely playing a key role.

445 In situ, the cyanobacteria of Pozo Bravo likely produce ROS during OP, as evidenced by the
446 transcription of oxidative stress proteins like thioredoxins and peroxiredoxin-5 (AHP1) (Supp. Fig
447 S13). Even though we observed no net H_2O_2 production, gross rates are likely very high, supported by
448 the large sink capacity of the mat revealed by the addition of H_2O_2 (Supp. Fig S8). Further ROS
449 formation from increasing light radiation through the day could be aggravated by 1) abiotic reactions
450 with iron and UV light [58], 2) singlet oxygen production during photosystem repair [59,60], and 3)
451 ROS produced due to arsenic oxidation, as proposed under physiological conditions by del Razo
452 (2001) [61]:

453 $H_3AsO_3 + 2H_2O + O_2 \rightarrow H_3AsO_4 + H_2O_2$ ($\Delta G°$=-40.82 kcal/mol) (2)

454 At noon, during maximum illumination, the sum of H_2O_2 production from OP and plausibly from
455 abiotic As(III) oxidation (Eq. 2) exceeds sink strength and net production of H_2O_2 becomes
456 measurable.

457 It is well documented that ROS can lead to the inhibition or complete interruption of OP to avoid
458 further ROS formation [62]. In Laguna Pozo Bravo, OP by cyanobacteria in the bottom layer, which
459 contains Chl-*f* (red in Fig 1), ceases after H_2O_2 is produced. OP is then replaced by oxidation of As(III)
460 under light targeting these Chl *f* cyanobacteria – an intriguing strategy to circumvent two problems
461 simultaneously: intracellular ROS production linked to OP and extracellular ROS production linked to
462 the presence of As(III) (Eq. 2). Cyanobacterial As(III)-driven AP is supported by a line of indirect

463 evidence. Most prominently, As(III) was oxidized under exposure to wavelengths exclusively targeting
464 oxygenic phototrophs. Also, DCMU did not inhibit this light-driven As(III) oxidation. Thus, oxidation
465 with photosynthetically produced O_2 can be excluded. The lack of inhibition by DCMU provides
466 additional information about the mechanisms behind As(III) oxidation. Specifically, it suggests that
467 electrons derived from As(III) oxidation enter the photosynthetic electron transport chain
468 downstream of PSII (Supp. Fig S17). This is because DCMU inhibits electron transfer at the acceptor
469 side of PSII. The specific enzymes involved in As(III)-driven AP in cyanobacteria, however, remain
470 unclear from the metagenomic and -transcriptomic data.

471 Neither As(III) concentration nor the light available to PSI regulate the transitions between
472 photosynthetic modes in the Chl *f* cyanobacteria. Instead, the shift in cyanobacterial photosynthetic
473 mode occurs exclusively under conditions of high light and in the presence of arsenic, resulting in an
474 accumulation of local ROS concentrations, resembling a stress response. Notably, As(III)-driven AP in
475 the Chl *a* cyanobacteria is regulated fundamentally different, i.e., it is not linked to the abundance of
476 H_2O_2. OP in incubations targeting Chl *a* only began after As(III) was depleted, indicating a regulation
477 by electron donor availability in Chl a cyanobacteria, analogous to observations in cyanobacteria
478 performing sulfide-driven photosynthesis [14]. To confidently test this hypothesis, however, it would
479 also be necessary to show photosynthetic As(III) oxidation in cyanobacterial isolates, rather than in
480 microbial mats.

481 The transitions from OP to AP could only be measured by supplementation with surplus arsenic. In
482 situ, however, almost no As(III) was measurable at noon. Yet, the interruption of OP and in situ gene
483 transcription of As(V) reductases (*ars*C) and As(III) oxidases (*aioA, aioB*) indicate that As(III) oxidation
484 was likely still occurring – in an active, yet cryptic, redox cycle. The source of As(III) for AP can only be
485 the reduction of the highly abundant As(V). Accordingly, *arsC* transcription was high during daylight
486 hours in the metatranscriptome (Fig 7a), and process rate measurements clearly showed that rates
487 were in the range of AP rates. Further, As(V) reduction rates were linearly dependent on
488 concentration within the measured range (up to ~19 µM) and did not yet saturate according to

Michaelis-Menten kinetics (Fig 4d). Such first order process suggests low-affinity enzymes, which are most efficient during the day at high As(V) levels.

To summarize, we propose that during the morning (dawn-10 am), both layers of cyanobacteria perform OP, while some Alphaproteobacteria (e.g. Rhodobacterales) begin with As(III)-AP (Fig 8). Through the mat, other Alphaproteobacteria, as well as Gammaproteobacteria, begin the reduction of intracellular As(V), resulting in As(V) reduction throughout the entire mat. ROS damage response appears to take place starting in the morning. During the late morning (10 am-12 pm), both layers of cyanobacteria continue doing OP even though As(III) is still present in the porewater. Then ROS accumulation is aggravated by increasing sunlight intensity combined with the presence of As(III). This could be due to spontaneous oxidation (eq. 2) , and/or ROS production during As(III)-affected OP. In the early afternoon (12 pm -3 pm), the increased ROS damage triggers cyanobacteria in the deeper layer to stop OP and to transition to As(III)-driven AP. In the late afternoon (3pm to sunset), less ROS is produced in the top layer due to lower OP, and the lower Chl *f* cyanobacteria switch back to OP. It remains unclear why the upper cyanobacteria do not follow the same photosynthetic switch as the lower zone, but instead keep performing OP during the afternoon, albeit at diminished rates (green mat layer in Fig 1a). A plausible explanation could be the lower As(III) supply from the deeper layers.

Fig 8. Proposed metabolic activities driving arsenic cycling through a diel cycle within Pozo Bravo microbial mats. These are based on pooling insights from hyperspectral imaging, process rate measurements and metatranscriptomic analyses. Reactive oxygen species (ROS) production during the morning, afternoon and late afternoon is indicated with grey clouds.

These dynamics have implications for the regulation of OP throughout the Precambrian. Due to the generally reducing environment in the Precambrian, and frequent input of arsenic from volcanic activity, As(III) was abundant in ancient oceans and was likely to be an electron donor for ancient AP [3,63,64]. Although some evidence pointing toward AP in *Oscillatoria* sp. arose in studies of microbial mats from Mono Lake, California [5], As(III)-driven AP has not been conclusively reported in cyanobacteria. This study yields valuable experimental data as another step in a long line of evidence

for the hidden metabolic capabilities of cyanobacteria [19,65,66]. While the exact metabolic mechanisms behind the interruption of OP and transition to As(III)-driven AP are yet to be understood, here we clearly show that arsenic has a fundamental effect on the diel O_2 budget of cyanobacterial mats by tempering O_2 export. Additionally, the cryptic cycling of arsenic in Laguna Pozo Bravo may showcase the hidden, yet quick and important, nature of arsenic metabolisms.

4. Methods

4.1. Field measurements and sampling

Field measurements and sampling were conducted in Laguna Pozo Bravo (25° 30' 58" S, 67° 34' 42" W), in the Salar de Antofalla, Argentina in late February 2019 and January 2023 at an elevation of 3330 m. To assess diel dynamics of oxygen and H_2S within the mat, we continuously measured depth profiles of concentration on two consecutive days, in two spots of the mat. The microsensors (H_2S and Clark-type O_2 with <50 µM tip width) were constructed, calibrated and used as previously described [67–70]. Vertical profiles were measured simultaneously by attaching the microsensors to a multi-sensor holder, yielding a distance between tips of ~0.5 cm. Electricity was provided by a portable generator. Using O_2 microsensor measurements, we calculated the net rates of OP as the difference in the fluxes into and out of the two photosynthetically active zones.

In parallel with the microsensor measurements, subsamples of the mat were regularly taken for porewater extraction and meta-omics. Cores for porewater extraction (2.5 cm inner diameter) were sampled in triplicate every three hours from 1 am until 6 pm. Porewater was immediately extracted from the cores (2.5 cm ID, up to 6 cm depth) at 1 cm intervals using rhizones (Rhizosphere Research Products, NL). An aliquot of 500 µL porewater was instantly frozen with liquid nitrogen and stored and transported in a dry shipper until arsenic speciation analysis using an ICP-MS as previously described [49] (Supp. Methods 1.1).

Additional sediment cores for meta-omics (2.5 cm inner diameter, up to 4 cm depth) were sampled in triplicates every three hours. The microbial mat was rapidly and carefully cut into four pieces per

core that were instantly frozen in liquid nitrogen for metagenomic and metatranscriptomic analyses. A few additional cores were frozen intact for hyperspectral imaging (Supp. Methods 1.2). Further, 10 x 5 cm pieces of mat with ~0.5 cm underlying sediment were stored in plastic containers for transport and maintained in mesocosms at ~700 µmol photons m^{-2} s^{-1} underneath a water column with a salinity of ~137 g L^{-1} (TropicMarine artificial saltwater), constantly circulated to maintain a temperature of 21°C, until ex-situ measurements.

Temperature of air and water above the mat were recorded using HOBO loggers (Onset Computer Corp., MA). Measurements of light intensity failed due to rapid oversaturation of the sensor signal in the morning. Occasionally, pH measurements in the water column were taken using a Mettler Toledo pH meter. Salinity was measured with an Atago refractometer.

4.2. Assessment of diel H_2O_2 dynamics

To assess the effect of light and arsenic on net O_2 production and H_2O_2 dynamics in the mat, we subsampled microbial mat pieces (~ 2.5×2.5 cm) from the laboratory mesocosms and continuously measured O_2 and H_2O_2 depth profiles during simulated diel light cycles, in the absence and presence of dissolved arsenic. Mat pieces were cut and fixed with low-melting agarose (1%) to the bottom of glass dishes. Circular flow was established with the same hypersaline water (TropicMarine artificial saltwater approximately 137 g L^{-1}) used for regular maintenance of the mats, and adjusted using a peristaltic pump (Minipuls 3 Abimed, Gilson). Diel cycles were simulated using halogen light sources (KL 2500 and KL 1500, Schott). Microsensors (H_2O_2, and O_2 with 80-120 µM tip diameter) were constructed, calibrated and used as previously described [67–70]. Concentration-depth profiles were performed under three light conditions: dark, 500 and 1000 µmol photons m^{-2} s^{-1}. First, profiles were measured without supplementing As(V), assuming that most arsenic had been washed out after four months of lab maintenance. Then As(V) was added to the overlying water column to a final concentration approximately 10 µM, mimicking the environmental As(V) maximum. After As(V) addition, mats were left undisturbed overnight to enable the diffusion of arsenic into the mat, and

566 diel profiling began in the morning. Diel profiling was also performed in As(V)-supplemented mats
567 after addition of DCMU, an inhibitor of OP, and after autoclaving the mat as an abiotic control.

568 Depth-integrated rates of net O_2 and H_2O_2 production were calculated from the concentration depth
569 profiles by considering Fick's second law of diffusion. First, local volumetric net rates were calculated
570 as the second derivative of concentration multiplied by the diffusion coefficient corrected for
571 temperature and salinity. Volumetric depth rates were then integrated over the uppermost 5 mm of
572 the mat.

573 4.3. Assessment of arsenic cycling rates in batch incubations

574 To assess the dependency of light quality on arsenic cycling, small subsamples of microbial mats were
575 incubated under As(V), As(III), and LED lights targeting distinct groups of phototrophs. Hypersaline
576 water (TropicMarine artificial saltwater ~137 g L^{-1}) was deoxygenated by bubbling with helium,
577 vigorously shaking, then removing gas bubbles, repeated five times. Subsamples cut from microbial
578 mats (~200 mg) using 8 mm width cores (surface area 0.5 cm^2) were inserted into 3 mL gastight glass
579 vials with a septum cap (exetainers, Labco) which were later filled completely with deoxygenated
580 hypersaline saltwater. Then they were placed into containers on shakers, with constant flow of
581 temperature-regulated water. The incubations were subjected to 8-hour cycles of light with various
582 different spectral quality, followed by 8 hours of darkness. Controls were placed under constant
583 darkness. All light treatments were repeated with the addition of 5 µL DCMU solution (5 mM) to
584 inhibit oxygenic photosynthesis.

585 The light treatments were chosen at specific wavelengths to target different groups of phototrophs.
586 LEDs with an emission maximum (λ_{max}) at 690 nm (hexagonal high-power LEDs from Roithner
587 Lasertechnik, Vienna; Supp. Fig S18) were used to specifically target Chl *a*, i.e., the light harvesting
588 pigment of most cyanobacteria for photosystem I and the central pigment in the reaction center of
589 both photosystems. Since an unexpected absorption maximum was found at 715 nm in the lower
590 cyanobacterial layer, we also used LEDs in the far-red range of the spectrum with λ_{max} = 715 nm to

target cyanobacterial Chl *f*, which can likely act as antenna in both photosystems [11,71]. Additionally, we used λ_{max} = 810 to target BChl *a* of purple anoxygenic bacteria, and full-spectrum white light to target all phototrophs.

Every three hours, three incubation vials per treatment were removed for measurements. First, oxygen in each exetainer was measured with a microsensor, then 2 mL of the overlying water were filtered. From the filtered water, 1 mL was fixed with 4 mL 2% zinc acetate for total dissolved sulfide measurements, and 1 mL was fixed with 15.53 µL fixing solution and flash frozen for arsenic measurements. Fixing solution for arsenic measurements was made by mixing 27 mL of concentrated HNO_3 diluted 1:2 with ultrapure water and 100 mL fresh DTPA solution. The DTPA solution was made by mixing 6.75 mL ultrapure water, 6.75 mL concentrated HNO_3 and 50 mL of 40% premade DTPA*Na_5 solution (Sigma Aldrich, CAS 140-01-2). Sulfide was later measured as previously described [72], and arsenic was measured colorimetrically based on Castillejos Sepúlveda et al. (2022), with modifications to calculations due to the high salinity and absence of phosphate (Supp. Methods 1.2).

4.4. Metagenomics

A piece of microbial mat collected in situ at 12:30 pm, following the procedure described above, was sliced into the four distinct layers (crust, green, red, brown) and sent to the Max Planck Genome Center (MPGC, Cologne, Germany) for processing. DNA extraction was performed using the DNeasy PowerSoil Pro Kit (Qiagen). An Illumina-compatible library was prepared with NEB Ultra II DNA kit (NEB) and each library was shotgun sequenced with Illumina HiSeq3000 (2 x 150 bp, paired-end read mode). The crust and brown layers were sequenced at a depth of 6.8 million reads, while the green and red layers were sequenced at a depth of 34 million reads to target cyanobacteria, which are notoriously difficult to sequence.

Raw sequences were quality-trimmed with Trimmomatic v.0.38[73], and assembled with MEGAHIT v.1.2.9[74]. Initially, a co-assembly of all samples was used, but due to low cyanobacterial read depth, a second assembly was prepared using only reads from the green layer of the microbial mat.

Both assemblies were later processed using the same workflow, but the second assembly was only used for analysis of cyanobacteria.

Samples were mapped onto the assembly with Bowtie2 v.2.4.5 [75]. Gene calling was performed with Prodigal v.2.6.3 [76], and the resulting gene calls were annotated in anvio v.7.1 [77] using the KEGG KOfam v.95.0 [78] and COG v.2020 [79] databases with DIAMOND v.0.9.14 [80] search. Interproscan v.78 [81,82] was used for further annotations with the following databases: CATH-Gene3D v.4.2.0 [83], CDD v.3.17 [84], HAMAP v.2020_01 [85], PANTHER v.14.1 [86], Pfam v.32.0 [87], PIRSF v.3.02 [88], PRINTS v.42.0 [89], PROSITE Patterns and PROSITE Profiles v.2019_11 [90], SMART v.7.1 [91], SFLD v.4 [92], SUPERFAMILY v.1.75 [93] and TIGRFAMs v.15.0 [94]. Genes related to arsenic, photosynthesis, glutaredoxins, and thioredoxins were manually selected and annotated based on consensus from the automatically-generated annotations, using BLASTx v.2.2.31 [95] to resolve discrepancies.

Metagenomic analyses were initially focused on genes that could result in redox changes, before binning was performed to assign genes to distinct bacterial taxa.

Automatic binning was done with MetaBAT2 v.2.15 [96] on the large co-assembly and MaxBin2 2.2.7 [97] on the second assembly. In both cases, bins were manually refined in anvio. Taxonomy was assigned to bins using GTDB-TK v.95.0 [98,99] within anvio. The relative abundance of each bin was calculated using coverM v. 0.4.0 [100] and plotted using ggplot2 [101] in R v. 4.0.3 [102].

4.5. Metatranscriptomics

Microbial mat samples collected following the procedure described above in situ at 1:00 am, 9:40 am, 12:30 pm, 3:15 pm, and 6:30 pm were sent to Max Planck Genome Center (MPGC, Cologne, Germany) for processing. RNA was isolated using Quick-DNA/RNA Miniprep Plus Kit (Zymo Research). Next, an Illumina-compatible library was prepared with the kit Universal Prokaryotic RNA-Seq incl. Prokaryotic AnyDeplete for rRNA depletion (Tecan Genomics). Each sample was shotgun-sequenced with Illumina HiSeq3000 (2x150 bp, paired-end read mode) at depths ranging from 35.5

641 million to 51 million reads. Raw sequences were quality trimmed with Trimmomatic, then mapped
642 onto the metagenomic assemblies with BBmap v38.73 [103], and used featureCounts from Rsubread
643 v. 1.22.2 to obtain counts of each gene per metatranscriptomic sample. To compare gene
644 transcription across samples, counts of each gene call were normalized by calculating Transcripts Per
645 Million (TPM) as previously described [45]. The TPM of all gene calls annotated with the same
646 function (i.e.- the same gene name) were summed, and used to make heatmaps with Pheatmap
647 v.1.0.12 [104] in R.

648 Data availability

649 Data has been submitted to the EMBL Nucleotide Sequence Database (ENA). Metagenomic and
650 metatranscriptomic raw reads, as well as cyanobacterial metagenome-assembled genomes described
651 in Supp. Figure S15 and Supp. Table S4, can be found under project number PRJEB41764.
652 Metagenome-assembled genomes from the co-assembly (Figs 2,3,7, Supp. Fig S13-14 and Supp.
653 Table S3) can be found under project number PRJEB73824.

654 Acknowledgements

655 We would like to thank Secretaría de Medio Ambiente de la Provincia de Catamarca for providing the
656 research permit (Expte.EX-2022-02222431-CAT-DPB#SEAS), and Secretaría de Política Ambiental en
657 Recursos Naturales, Ministerio de Ambiente y Desarrollo Sostenible de la Nación Argentina for
658 providing the certificate of compliance (Title: IF-2023-65966642-APN-SPARN#MAD, UId: ABSCH-IRCC-
659 AR-264943-1) and the export certificate for genetic resources (CE-2023-69835755-APN-
660 SPARN#MAD). We would like to express our gratitude to Luis Ahumada for his assistance during the
661 field campaigns, and the native communities of Antofalla, El Peñón, and Antofagasta de la Sierra for
662 their valuable support. The authors also thank the laboratory technicians in the Microsensor working
663 group, the mechanical workshop in MPI Bremen, David Benito Merino, Marit van Erk, Britta Planer-
664 Friedrich, Martina Alisch, and Boran Kartal for their help with labwork, advice, and laboratory
665 equipment.

References

1. Nisbet EG, Fowler CMR. The Early History of Life. Treatise on Geochemistry. Elsevier; 2003. pp. 1–39. doi:10.1016/B0-08-043751-6/08166-4

2. Sleep NH. The Hadean-Archaean Environment. Cold Spring Harb Perspect Biol. 2010;2: a002527–a002527. doi:10.1101/cshperspect.a002527

3. Oremland RS, Saltikov CW, Wolfe-Simon F, Stolz JF. Arsenic in the evolution of earth and extraterrestrial ecosystems. Geomicrobiol J. 2009;26: 522–536. doi:10.1080/01490450903102525

4. Smedley P., Kinniburgh D. A review of the source, behaviour and distribution of arsenic in natural waters. Appl Geochemistry. 2002;17: 517–568. doi:10.1016/S0883-2927(02)00018-5

5. Kulp TR, Hoeft SE, Asao M, Madigan MT, Hollibaugh JT, Fisher JC, et al. Arsenic(III) Fuels Anoxygenic Photosynthesis in Hot Spring Biofilms from Mono Lake, California. Science (80-). 2008;321: 967–970. doi:10.1126/science.1160799

6. Slyemi D, Bonnefoy V. How prokaryotes deal with arsenic. Environ Microbiol Rep. 2012;4: 571–586. doi:10.1111/j.1758-2229.2011.00300.x

7. Castenholz RW. Phototrophic Bacteria Under UV Stress. In: Seckbach J, editor. Origins. Dordrecht: Kluwer Academic Publishers; 2004. pp. 445–461. doi:10.1007/1-4020-2522-X_27

8. Averina S, Velichko N, Senatskaya E, Pinevich A. Far-red light photoadaptations in aquatic cyanobacteria. Hydrobiologia. Springer International Publishing; 2018. pp. 1–17. doi:10.1007/s10750-018-3519-x

9. Gan F, Bryant DA. Adaptive and acclimative responses of cyanobacteria to far-red light. Environmental Microbiology. John Wiley & Sons, Ltd; 2015. pp. 3450–3465. doi:10.1111/1462-2920.12992

10. Gan F, Shen G, Bryant DA. Occurrence of far-red light photoacclimation (FaRLiP) in diverse cyanobacteria. Life. 2015;5: 4–24. doi:10.3390/life5010004

11. Gisriel CJ, Shen G, Ho MY, Kurashov V, Flesher DA, Wang J, et al. Structure of a monomeric photosystem II core complex from a cyanobacterium acclimated to far-red light reveals the functions of chlorophylls d and f. J Biol Chem. 2022;298: 101424. doi:10.1016/J.JBC.2021.101424/ATTACHMENT/E0177B24-B0ED-4877-814E-AD8491135B45/MMC2.ZIP

12. Padan E. Facultative Anoxygenic Photosynthesis in Cyanobacteria. Annu Rev Plant Physiol. 1979;30: 27–40. doi:10.1146/annurev.pp.30.060179.000331

13. Grim SL, Dick GJ. Photosynthetic Versatility in the Genome of Geitlerinema sp. PCC 9228 (Formerly Oscillatoria limnetica 'Solar Lake'), a Model Anoxygenic Photosynthetic Cyanobacterium. Front Microbiol. 2016;7. doi:10.3389/fmicb.2016.01546

14. Klatt JM, Al-Najjar MAA, Yilmaz P, Lavik G, de Beer D, Polerecky L. Anoxygenic Photosynthesis Controls Oxygenic Photosynthesis in a Cyanobacterium from a Sulfidic Spring. Kostka JE, editor. Appl Environ Microbiol. 2015;81: 2025–2031. doi:10.1128/AEM.03579-14

15. Trinugroho JP, Bečková M, Shao S, Yu J, Zhao Z, Murray JW, et al. Chlorophyll f synthesis by a super-rogue photosystem II complex. Nature Plants. Nature Publishing Group; 2020. pp. 238–244. doi:10.1038/s41477-020-0616-4

16. Cardona T, Murray JW, Rutherford AW. Origin and Evolution of Water Oxidation before the

Last Common Ancestor of the Cyanobacteria. Mol Biol Evol. 2015;32: 1310–1328. doi:10.1093/molbev/msv024

17. Cohen Y, Jørgensen BB, Revsbech NP, Poplawski R. Adaptation to Hydrogen Sulfide of Oxygenic and Anoxygenic Photosynthesis among Cyanobacteria. Appl Environ Microbiol. 1986;51: 398–407. doi:10.1128/aem.51.2.398-407.1986

18. Kelly DJ, Dow CS. Microbial Photosynthesis. Wang Q, editor. Compr Biotech, The Princip, Appl and Regal of Biotechnol in Ind, Agric and Med. Singapore: Springer Singapore; 2020. doi:10.1007/978-981-15-3110-1

19. Nagy CI, Vass I, Rákhely G, Vass IZ, Tóth A, Duzs A, et al. Coregulated genes link sulfide:quinone oxidoreductase and arsenic metabolism in Synechocystis sp. strain PCC6803. J Bacteriol. 2014;196: 3430–40. doi:10.1128/JB.01864-14

20. Rascovan N, Maldonado J, Vazquez MP, Eugenia Farías M. Metagenomic study of red biofilms from Diamante Lake reveals ancient arsenic bioenergetics in haloarchaea. ISME J. 2016;10: 299–309. doi:10.1038/ismej.2015.109

21. Sancho-Tomás M, Somogyi A, Medjoubi K, Bergamaschi A, Visscher PT, van Driessche AES, et al. Geochemical evidence for arsenic cycling in living microbialites of a High Altitude Andean Lake (Laguna Diamante, Argentina). Chem Geol. 2020;549: 119681. doi:10.1016/j.chemgeo.2020.119681

22. Sancho-Tomás M, Somogyi A, Medjoubi K, Bergamaschi A, Visscher PT, Van Driessche AES, et al. Distribution, redox state and (bio)geochemical implications of arsenic in present day microbialites of Laguna Brava, Salar de Atacama. Chem Geol. 2018;490: 13–21. doi:10.1016/j.chemgeo.2018.04.029

23. Kurth D, Amadio A, Ordoñez OF, Albarracín VH, Gärtner W, Farías ME. Arsenic metabolism in high altitude modern stromatolites revealed by metagenomic analysis. Sci Rep. 2017;7: 1024. doi:10.1038/s41598-017-00896-0

24. Visscher PT, Gallagher KL, Bouton A, Farias ME, Kurth D, Sancho-Tomás M, et al. Modern arsenotrophic microbial mats provide an analogue for life in the anoxic Archean. Commun Earth Environ. 2020;1: 1–10. doi:10.1038/s43247-020-00025-2

25. Lencina AI, Soria MN, Gomez FJ, Gérard E, Farias ME. Composite microbialites: Thrombolite, dendrolite, and stromatolite associations in a modern environment, Pozo Bravo lake, Salar de Antofalla, Catamarca Puna, Argentina. J Sediment Res. 2021;91: 1305–1330. doi:10.2110/jsr.2020.166

26. Vignale FA, Lencina AI, Stepanenko TM, Soria MN, Saona LA, Kurth D, et al. Lithifying and Non-Lithifying Microbial Ecosystems in the Wetlands and Salt Flats of the Central Andes. Microb Ecol. 2022;83: 1–17. doi:10.1007/s00248-021-01725-8

27. Farías ME, Villafañe PG, Lencina AI. Integral prospection of Andean microbial ecosystem project. Microb Ecosyst Cent Andes Extrem Environ biofilms, Microb mats, microbialites endoevaporites. 2020; 245–260.

28. Nisbet EG, Fowler CMR. Archaean metabolic evolution of microbial mats. Proc R Soc B Biol Sci. 1999;266: 2375–2382. doi:10.1098/rspb.1999.0934

29. Yacobi YZ, Köhler J, Leunert F, Gitelson A. Phycocyanin-specific absorption coefficient: Eliminating the effect of chlorophylls absorption. Limnol Oceanogr Methods. 2015;13: 157–168. doi:10.1002/lom3.10015

30. Jørgensen BB, Cohen Y, des Marais DJ, Jorgensen BB, Cohen Y, des Marais DJ. Photosynthetic

752 action spectra and adaptation to spectral light distribution in a benthic cyanobacterial mat.
753 Appl Environ Microbiol. 1987;53: 879–886. doi:10.4319/lo.1992.37.8.1813

754 31. Stomp M, Huisman J, Stal LJ, Matthijs HCP. Colorful niches of phototrophic microorganisms
755 shaped by vibrations of the water molecule. ISME J. 2007;1: 271–282.
756 doi:10.1038/ismej.2007.59

757 32. Miller LC, Martin DS, Liu L-N, Canniffe DP, Miller LC, Canniffe · D P, et al. Composition,
758 Organisation and Function of Purple Photosynthetic Machinery. Microb Photosynth. 2020;
759 73–114. doi:10.1007/978-981-15-3110-1_4

760 33. Blankenship RE, Olson JM, Miller M. Antenna Complexes from Green Photosynthetic Bacteria.
761 Anoxygenic Photosynthetic Bacteria. Dordrecht: Kluwer Academic Publishers; 1995. pp. 399–
762 435. doi:10.1007/0-306-47954-0_20

763 34. Sawicki A, Chen M, Sawicki A, Chen · M. Molecular Mechanism of Photosynthesis Driven by
764 Red-Shifted Chlorophylls. Microb Photosynth. 2020; 3–42. doi:10.1007/978-981-15-3110-1_1

765 35. Rosen BP. Biochemistry of arsenic detoxification. FEBS Lett. 2002;529: 86–92.
766 doi:http://dx.doi.org/10.1016/S0014-5793(02)03186-1

767 36. Yang HC, Fu HL, Lin YF, Rosen BP. Pathways of Arsenic Uptake and Efflux. Current Topics in
768 Membranes. Academic Press Inc.; 2012. pp. 325–358. doi:10.1016/B978-0-12-394390-
769 3.00012-4

770 37. Willsky GR, Malamy MH. Effect of arsenate on inorganic phosphate transport in Escherichia
771 coli. J Bacteriol. 1980;144: 366–374. doi:10.1128/jb.144.1.366-374.1980

772 38. Elias M, Wellner A, Goldin-Azulay K, Chabriere E, Vorholt JA, Erb TJ, et al. The molecular basis
773 of phosphate discrimination in arsenate-rich environments. Nature. 2012;491: 134–137.
774 doi:10.1038/nature11517

775 39. Saona LA, Soria M, Durán-Toro V, Wörmer L, Milucka J, Castro-Nallar E, et al. Phosphate-
776 Arsenic Interactions in Halophilic Microorganisms of the Microbial Mat from Laguna
777 Tebenquiche: from the Microenvironment to the Genomes. Microb Ecol. 2021;81: 941–953.
778 doi:10.1007/s00248-020-01673-9

779 40. Ordóñez E, Van Belle K, Roos G, De Galan S, Letek M, Gil JA, et al. Arsenate reductase,
780 mycothiol, and mycoredoxin concert thiol/disulfide exchange. J Biol Chem. 2009;284: 15107–
781 15116. Available: https://pubmed.ncbi.nlm.nih.gov/19286650/

782 41. Jiang Z, Shen X, Shi B, Cui M, Wang Y, Li P. Arsenic Mobilization and Transformation by
783 Ammonium-Generating Bacteria Isolated from High Arsenic Groundwater in Hetao Plain,
784 China. Int J Environ Res Public Health. 2022;19: 9606. doi:10.3390/ijerph19159606

785 42. Rascovan N, Maldonado J, Vazquez MP, Eugenia Farías M. Metagenomic study of red biofilms
786 from Diamante Lake reveals ancient arsenic bioenergetics in haloarchaea. ISME J. 2016;10:
787 299–309. doi:10.1038/ismej.2015.109

788 43. Ordoñez OF, Lanzarotti E, Kurth D, Cortez N, Farías ME, Turjanski AG. Genome comparison of
789 two Exiguobacterium strains from high altitude andean lakes with different arsenic resistance:
790 identification and 3D modeling of the Acr3 efflux pump. Front Environ Sci. 2015;3.
791 doi:10.3389/fenvs.2015.00050

792 44. Hoeft McCann S, Boren A, Hernandez-Maldonado J, Stoneburner B, Saltikov C, Stolz J, et al.
793 Arsenite as an Electron Donor for Anoxygenic Photosynthesis: Description of Three Strains of
794 Ectothiorhodospira from Mono Lake, California and Big Soda Lake, Nevada. Life. 2016;7: 1.
795 doi:10.3390/life7010001

45. Wagner GP, Kin K, Lynch VJ. Measurement of mRNA abundance using RNA-seq data: RPKM measure is inconsistent among samples. Theory Biosci. 2012;131: 281–285. doi:10.1007/s12064-012-0162-3

46. Páez-Espino D, Tamames J, De Lorenzo V, Cánovas D. Microbial responses to environmental arsenic. BioMetals. 2009;22: 117–130. doi:10.1007/s10534-008-9195-y

47. Silver S, Phung LT. Genes and enzymes involved in bacterial oxidation and reduction of inorganic arsenic. Appl Environ Microbiol. 2005;71: 599–608. doi:10.1128/AEM.71.2.599-608.2005

48. de Beer D, Meyer V, Klatt J, Li T. Photosynthesis under very high oxygen concentrations in dense microbial mats and biofilms. bioRxiv. 2018; 335299. doi:10.1101/335299

49. Castillejos Sepúlveda A, Gatti LM, Kerl CF, Chennu A, Klatt JM. Arsenic speciation analysis in porewater by a novel colorimetric assay. Sci Total Environ. 2022;827: 154155. doi:10.1016/j.scitotenv.2022.154155

50. Oremland RS, Hoeft SE, Santini JM, Bano N, Hollibaugh RA, Hollibaugh JT. Anaerobic oxidation of arsenite in Mono Lake water and by a facultative, arsenite-oxidizing chemoautotroph, strain MLHE-1. Appl Environ Microbiol. 2002;68: 4795–802. doi:10.1128/AEM.68.10.4795

51. Zhang J, Zhou W, Liu B, He J, Shen Q, Zhao FJ. Anaerobic arsenite oxidation by an autotrophic arsenite-oxidizing bacterium from an arsenic-contaminated paddy soil. Environ Sci Technol. 2015;49: 5956–5964. doi:10.1021/es506097c

52. Franks J, Stolz JF. Flat laminated microbial mat communities. Earth-Science Rev. 2009;96: 163–172. doi:10.1016/J.EARSCIREV.2008.10.004

53. Flores-Kim J, Darwin AJ. The Phage Shock Protein Response. Annu Rev Microbiol. 2016;70: 83–101. doi:10.1146/ANNUREV-MICRO-102215-095359

54. Junglas B, Huber ST, Heidler T, Schlösser L, Mann D, Hennig R, et al. PspA adopts an ESCRT-III-like fold and remodels bacterial membranes. Cell. 2021;184: 3674-3688.e18. doi:10.1016/J.CELL.2021.05.042

55. Sheridan KJ, Duncan EJ, Eaton-Rye JJ, Summerfield TC. The diversity and distribution of D1 proteins in cyanobacteria. Photosynth Res. 2020;145: 111–128. doi:10.1007/s11120-020-00762-7

56. Lubitz W, Lendzian F, Bittl R. Radicals, radical pairs and triplet states in photosynthesis. Acc Chem Res. 2002;35: 313–320. doi:10.1021/AR000084G/ASSET/IMAGES/LARGE/AR000084GF00007.JPEG

57. Budinoff CR, Hollibaugh JT. Arsenite-dependent photoautotrophy by an Ectothiorhodospira-dominated consortium. ISME J. 2008;2: 340–343. doi:10.1038/ismej.2007.115

58. Blokhina O, Virolainen E, Fagerstedt K V. Antioxidants, oxidative damage and oxygen deprivation stress: A review. Annals of Botany. 2003. pp. 179–194. doi:10.1093/aob/mcf118

59. Hakala-Yatkin M, Sarvikas P, Paturi P, Mäntysaari M, Mattila H, Tyystjärvi T, et al. Magnetic field protects plants against high light by slowing down production of singlet oxygen. Physiol Plant. 2011;142: 26–34. doi:10.1111/j.1399-3054.2011.01453.x

60. Marais A, Sinayskiy I, Petruccione F, Van Grondelle R. A quantum protective mechanism in photosynthesis. Sci Reports 2015 51. 2015;5: 1–8. doi:10.1038/srep08720

61. Del Razo LM, Quintanilla-Vega B, Brambila-Colombres E, Calderón-Aranda ES, Manno M, Albores A. Stress proteins induced by arsenic. Toxicol Appl Pharmacol. 2001;177: 132–148.

839 doi:10.1006/TAAP.2001.9291

840 62. Latifi A, Ruiz M, Zhang C-C. Oxidative stress in cyanobacteria. FEMS Microbiol Rev. 2009;33:
841 258–278. doi:10.1111/j.1574-6976.2008.00134.x

842 63. Jackson CR, Langner HW, Donahoe-Christiansen J, Inskeep WP, McDermott TR. Molecular
843 analysis of microbial community structure in an arsenite-oxidizing acidic thermal spring.
844 Environ Microbiol. 2001;3: 532–542. doi:10.1046/j.1462-2920.2001.00221.x

845 64. Lebrun E, Brugna M, Baymann F, Muller D, Lièvremont D, Lett M-C, et al. Arsenite oxidase, an
846 ancient bioenergetic enzyme. Mol Biol Evol. 2003;20: 686–93. doi:10.1093/molbev/msg071

847 65. Grim SL, Dick GJ. Photosynthetic versatility in the genome of Geitlerinema sp. PCC 9228
848 (Formerly Oscillatoria limnetica 'solar lake'), a model anoxygenic photosynthetic
849 cyanobacterium. Front Microbiol. 2016;7: 1–14. doi:10.3389/fmicb.2016.01546

850 66. Sforna MC, Philippot P, Somogyi A, Van Zuilen MA, Medjoubi K, Schoepp-Cothenet B, et al.
851 Evidence for arsenic metabolism and cycling by microorganisms 2.7 billion years ago. Nat
852 Geosci. 2014;7: 811–815. doi:10.1038/ngeo2276

853 67. De Beer D, Schramm A, Santegoeds CM, Kühl M, Kuhl M. A nitrite microsensor for profiling
854 environmental biofilms. Appl Environ Microbiol. 1997;63: 973–7. Available:
855 http://www.ncbi.nlm.nih.gov/pubmed/16535560

856 68. Jeroschewski P, Steuckart C, Kühl M. An Amperometric Microsensor for the Determination of
857 H 2 S in Aquatic Environments. Anal Chem. 1996;68: 4351–4357. doi:10.1021/ac960091b

858 69. Klatt JM, Meyer S, Häusler S, Macalady JL, De Beer D, Polerecky L. Structure and function of
859 natural sulphide-oxidizing microbial mats under dynamic input of light and chemical energy.
860 ISME J. 2016;10: 921–33. doi:10.1038/ismej.2015.167

861 70. Revsbech NP. An oxygen microsensor with a guard cathode. Limnology and Oceanography.
862 John Wiley & Sons, Ltd; 1989. pp. 474–478. doi:10.4319/lo.1989.34.2.0474

863 71. Tros M, Mascoli V, Shen G, Ho MY, Bersanini L, Gisriel CJ, et al. Breaking the Red Limit:
864 Efficient Trapping of Long-Wavelength Excitations in Chlorophyll-f-Containing Photosystem I.
865 Chem. 2021;7: 155–173. doi:10.1016/J.CHEMPR.2020.10.024

866 72. Cline JD. Spectrophotometric determination of hydrogren sulfide in natural waters. Limnol
867 Oceanogr. 1969;14: 454–458. doi:10.4319/lo.1969.14.3.0454

868 73. Bolger AM, Lohse M, Usadel B. Trimmomatic: A flexible trimmer for Illumina sequence data.
869 Bioinformatics. 2014;30: 2114–2120. doi:10.1093/bioinformatics/btu170

870 74. Li D, Liu C-M, Luo R, Sadakane K, Lam T-W. MEGAHIT: an ultra-fast single-node solution for
871 large and complex metagenomics assembly via succinct de Bruijn graph. Bioinformatics.
872 2015;31: 1674–1676. doi:10.1093/bioinformatics/btv033

873 75. Langmead B, Salzberg SL. Fast gapped-read alignment with Bowtie 2. Nat Methods. 2012;9:
874 357–359. doi:10.1038/nmeth.1923

875 76. Hyatt D, Chen GL, LoCascio PF, Land ML, Larimer FW, Hauser LJ. Prodigal: Prokaryotic gene
876 recognition and translation initiation site identification. BMC Bioinformatics. 2010;11: 1–11.
877 doi:10.1186/1471-2105-11-119

878 77. Eren AM, Esen OC, Quince C, Vineis JH, Morrison HG, Sogin ML, et al. Anvi'o: An advanced
879 analysis and visualization platformfor 'omics data. PeerJ. 2015;2015: e1319.
880 doi:10.7717/PEERJ.1319/SUPP-5

881 78. Aramaki T, Blanc-Mathieu R, Endo H, Ohkubo K, Kanehisa M, Goto S, et al. KofamKOALA:
882 KEGG Ortholog assignment based on profile HMM and adaptive score threshold. Valencia A,
883 editor. Bioinformatics. 2020;36: 2251–2252. doi:10.1093/bioinformatics/btz859

884 79. Tatusov RL, Galperin MY, Natale DA, Koonin E V. The COG database: a tool for genome-scale
885 analysis of protein functions and evolution. Nucleic Acids Res. 2000;28: 33.
886 doi:10.1093/NAR/28.1.33

887 80. Buchfink B, Xie C, Huson DH. Fast and sensitive protein alignment using DIAMOND. Nat
888 Methods. 2015;12: 59–60. doi:10.1038/nmeth.3176

889 81. Blum M, Chang HY, Chuguransky S, Grego T, Kandasaamy S, Mitchell A, et al. The InterPro
890 protein families and domains database: 20 years on. Nucleic Acids Res. 2021;49: D344–D354.
891 doi:10.1093/nar/gkaa977

892 82. Jones P, Binns D, Chang HY, Fraser M, Li W, McAnulla C, et al. InterProScan 5: Genome-scale
893 protein function classification. Bioinformatics. 2014;30: 1236–1240.
894 doi:10.1093/bioinformatics/btu031

895 83. Sillitoe I, Dawson N, Lewis TE, Das S, Lees JG, Ashford P, et al. CATH: Expanding the horizons of
896 structure-based functional annotations for genome sequences. Nucleic Acids Res. 2019;47:
897 D280–D284. doi:10.1093/nar/gky1097

898 84. Lu S, Wang J, Chitsaz F, Derbyshire MK, Geer RC, Gonzales NR, et al. CDD/SPARCLE: the
899 conserved domain database in 2020. - PubMed - NCBI. Nucleic Acids Res. 2020;48: D265–
900 D268. Available: https://academic.oup.com/nar/article-abstract/48/D1/D265/5645006

901 85. Pedruzzi I, Rivoire C, Auchincloss AH, Coudert E, Keller G, De Castro E, et al. HAMAP in 2015:
902 Updates to the protein family classification and annotation system. Nucleic Acids Res.
903 2015;43: D1064–D1070. doi:10.1093/nar/gku1002

904 86. Mi H, Muruganujan A, Ebert D, Huang X, Thomas PD. PANTHER version 14: More genomes, a
905 new PANTHER GO-slim and improvements in enrichment analysis tools. Nucleic Acids Res.
906 2019;47: D419–D426. doi:10.1093/nar/gky1038

907 87. Bateman A, Birney E, Durbin R, Eddy SR, Howe KL, Sonnhammer ELL. The Pfam protein
908 families database. Nucleic Acids Research. 2000. pp. 263–266. doi:10.1093/nar/28.1.263

909 88. Nikolskaya AN, Arighi CN, Huang H, Barker WC, Wu CH. PIRSF Family Classification System for
910 Protein Functional and Evolutionary Analysis. Evol Bioinforma. 2006;2: 117693430600200.
911 doi:10.1177/117693430600200033

912 89. Attwood TK, Coletta A, Muirhead G, Pavlopoulou A, Philippou PB, Popov I, et al. The PRINTS
913 database: A fine-grained protein sequence annotation and analysis resource-its status in
914 2012. Database. 2012;2012. doi:10.1093/database/bas019

915 90. Sigrist CCJA, Castro E De, … LC-N acids, 2012 undefined, de Castro E, Cerutti L, et al. New and
916 continuing developments at PROSITE. 2012;41: D344–D347. doi:10.1093/nar/gks1067

917 91. Letunic I, Bork P. 20 years of the SMART protein domain annotation resource. Nucleic Acids
918 Res. 2018;46: D493–D496. doi:10.1093/nar/gkx922

919 92. Brown S, Pegg S, Ojha S, Huang C, Ferrin TE, Babbitt PC. The Structure-Function Linkage
920 Database. FASEB J. 2006;20. doi:10.1096/fasebj.20.5.a899-c

921 93. Pandurangan AP, Stahlhacke J, Oates ME, Smithers B, Gough J. The SUPERFAMILY 2.0
922 database: A significant proteome update and a new webserver. Nucleic Acids Res. 2019;47:
923 D490–D494. doi:10.1093/nar/gky1130

924 94. Haft DH, Selengut JD, Richter RA, Harkins D, Basu MK, Beck E. TIGRFAMs and genome
925 properties in 2013. Nucleic Acids Res. 2013;41. doi:10.1093/nar/gks1234

926 95. Camacho C, Coulouris G, Avagyan V, Ma N, Papadopoulos J, Bealer K, et al. BLAST+:
927 Architecture and applications. BMC Bioinformatics. 2009;10: 1–9. doi:10.1186/1471-2105-10-
928 421/FIGURES/4

929 96. Kang DD, Li F, Kirton E, Thomas A, Egan R, An H, et al. MetaBAT 2: An adaptive binning
930 algorithm for robust and efficient genome reconstruction from metagenome assemblies.
931 PeerJ. 2019;2019: e7359. doi:10.7717/PEERJ.7359/SUPP-3

932 97. Wu Y-W, Simmons BA, Singer SW. MaxBin 2.0: an automated binning algorithm to recover
933 genomes from multiple metagenomic datasets. Bioinformatics. 2016;32: 605–607.
934 doi:10.1093/bioinformatics/btv638

935 98. Parks DH, Chuvochina M, Waite DW, Rinke C, Skarshewski A, Chaumeil P-A, et al. A
936 standardized bacterial taxonomy based on genome phylogeny substantially revises the tree of
937 life. Nat Biotechnol. 2018;36: 996–1004. doi:10.1038/nbt.4229

938 99. Chaumeil PA, Mussig AJ, Hugenholtz P, Parks DH. GTDB-Tk: a toolkit to classify genomes with
939 the Genome Taxonomy Database. Bioinformatics. 2020;36: 1925–1927.
940 doi:10.1093/BIOINFORMATICS/BTZ848

941 100. Woodcroft BJ, Newell R. wwood/CoverM: Read coverage calculator for metagenomics. Centre
942 for Microbiome Research, School of Biomedical Sciences, Faculty of Health, Queensland
943 University of Technology; 2021 [cited 22 Jul 2022]. Available:
944 https://github.com/wwood/CoverM#readme

945 101. Wickham H. ggplot2: Elegant Graphics for Data Analysis. Cham: Springer-Verlag New York;
946 2016. doi:10.1007/978-3-319-24277-4

947 102. R Core Team. R: A Language and Environment for Statistical Computing. Vienna, Austria; 2020
948 [cited 3 May 2023]. Available: https://www.r-project.org/

949 103. Bushnell B. BBMap short-read aligner, and other bioinformatics tools. 2015.

950 104. Kolde R. CRAN - Package pheatmap. In: https://cran.r-project.org/package=pheatmap
951 [Internet]. 2019 [cited 12 Jun 2022]. Available: https://cran.r-
952 project.org/web/packages/pheatmap/index.html

953 1. Nisbet EG, Fowler CMR. The Early History of Life. Treatise on Geochemistry. Elsevier; 2003. pp.
954 1–39. doi:10.1016/B0-08-043751-6/08166-4

955 2. Sleep NH. The Hadean-Archaean Environment. Cold Spring Harb Perspect Biol. 2010;2:
956 a002527–a002527. doi:10.1101/cshperspect.a002527

957 3. Oremland RS, Saltikov CW, Wolfe-Simon F, Stolz JF. Arsenic in the evolution of earth and
958 extraterrestrial ecosystems. Geomicrobiol J. 2009;26: 522–536.
959 doi:10.1080/01490450903102525

960 4. Smedley P., Kinniburgh D. A review of the source, behaviour and distribution of arsenic in

natural waters. Appl Geochemistry. 2002;17: 517–568. doi:10.1016/S0883-2927(02)00018-5

5. Kulp TR, Hoeft SE, Asao M, Madigan MT, Hollibaugh JT, Fisher JC, et al. Arsenic(III) Fuels Anoxygenic Photosynthesis in Hot Spring Biofilms from Mono Lake, California. Science (80-). 2008;321: 967–970. doi:10.1126/science.1160799

6. Slyemi D, Bonnefoy V. How prokaryotes deal with arsenic. Environ Microbiol Rep. 2012;4: 571–586. doi:10.1111/j.1758-2229.2011.00300.x

7. Castenholz RW. Phototrophic Bacteria Under UV Stress. In: Seckbach J, editor. Origins. Dordrecht: Kluwer Academic Publishers; 2004. pp. 445–461. doi:10.1007/1-4020-2522-X_27

8. Averina S, Velichko N, Senatskaya E, Pinevich A. Far-red light photoadaptations in aquatic cyanobacteria. Hydrobiologia. Springer International Publishing; 2018. pp. 1–17. doi:10.1007/s10750-018-3519-x

9. Gan F, Bryant DA. Adaptive and acclimative responses of cyanobacteria to far-red light. Environmental Microbiology. John Wiley & Sons, Ltd; 2015. pp. 3450–3465. doi:10.1111/1462-2920.12992

10. Gan F, Shen G, Bryant DA. Occurrence of far-red light photoacclimation (FaRLiP) in diverse cyanobacteria. Life. 2015;5: 4–24. doi:10.3390/life5010004

11. Gisriel CJ, Shen G, Ho MY, Kurashov V, Flesher DA, Wang J, et al. Structure of a monomeric photosystem II core complex from a cyanobacterium acclimated to far-red light reveals the functions of chlorophylls d and f. J Biol Chem. 2022;298: 101424. doi:10.1016/J.JBC.2021.101424/ATTACHMENT/E0177B24-B0ED-4877-814E-AD8491135B45/MMC2.ZIP

12. Padan E. Facultative Anoxygenic Photosynthesis in Cyanobacteria. Annu Rev Plant Physiol. 1979;30: 27–40. doi:10.1146/annurev.pp.30.060179.000331

13. Grim SL, Dick GJ. Photosynthetic Versatility in the Genome of Geitlerinema sp. PCC 9228

(Formerly Oscillatoria limnetica 'Solar Lake'), a Model Anoxygenic Photosynthetic Cyanobacterium. Front Microbiol. 2016;7. doi:10.3389/fmicb.2016.01546

14. Klatt JM, Al-Najjar MAA, Yilmaz P, Lavik G, de Beer D, Polerecky L. Anoxygenic Photosynthesis Controls Oxygenic Photosynthesis in a Cyanobacterium from a Sulfidic Spring. Kostka JE, editor. Appl Environ Microbiol. 2015;81: 2025–2031. doi:10.1128/AEM.03579-14

15. Trinugroho JP, Bečková M, Shao S, Yu J, Zhao Z, Murray JW, et al. Chlorophyll f synthesis by a super-rogue photosystem II complex. Nature Plants. Nature Publishing Group; 2020. pp. 238–244. doi:10.1038/s41477-020-0616-4

16. Cardona T, Murray JW, Rutherford AW. Origin and Evolution of Water Oxidation before the Last Common Ancestor of the Cyanobacteria. Mol Biol Evol. 2015;32: 1310–1328. doi:10.1093/molbev/msv024

17. Cohen Y, Jørgensen BB, Revsbech NP, Poplawski R. Adaptation to Hydrogen Sulfide of Oxygenic and Anoxygenic Photosynthesis among Cyanobacteria. Appl Environ Microbiol. 1986;51: 398–407. doi:10.1128/aem.51.2.398-407.1986

18. Kelly DJ, Dow CS. Microbial Photosynthesis. Wang Q, editor. Compr Biotech, The Princip, Appl and Regal of Biotechnol in Ind, Agric and Med. Singapore: Springer Singapore; 2020. doi:10.1007/978-981-15-3110-1

19. Nagy CI, Vass I, Rákhely G, Vass IZ, Tóth A, Duzs A, et al. Coregulated genes link sulfide:quinone oxidoreductase and arsenic metabolism in Synechocystis sp. strain PCC6803. J Bacteriol. 2014;196: 3430–40. doi:10.1128/JB.01864-14

20. Rascovan N, Maldonado J, Vazquez MP, Eugenia Farías M. Metagenomic study of red biofilms from Diamante Lake reveals ancient arsenic bioenergetics in haloarchaea. ISME J. 2016;10: 299–309. doi:10.1038/ismej.2015.109

21. Sancho-Tomás M, Somogyi A, Medjoubi K, Bergamaschi A, Visscher PT, van Driessche AES, et

1009 al. Geochemical evidence for arsenic cycling in living microbialites of a High Altitude Andean
1010 Lake (Laguna Diamante, Argentina). Chem Geol. 2020;549: 119681.
1011 doi:10.1016/j.chemgeo.2020.119681

1012 22. Sancho-Tomás M, Somogyi A, Medjoubi K, Bergamaschi A, Visscher PT, Van Driessche AES, et
1013 al. Distribution, redox state and (bio)geochemical implications of arsenic in present day
1014 microbialites of Laguna Brava, Salar de Atacama. Chem Geol. 2018;490: 13–21.
1015 doi:10.1016/j.chemgeo.2018.04.029

1016 23. Kurth D, Amadio A, Ordoñez OF, Albarracín VH, Gärtner W, Farías ME. Arsenic metabolism in
1017 high altitude modern stromatolites revealed by metagenomic analysis. Sci Rep. 2017;7: 1024.
1018 doi:10.1038/s41598-017-00896-0

1019 24. Visscher PT, Gallagher KL, Bouton A, Farias ME, Kurth D, Sancho-Tomás M, et al. Modern
1020 arsenotrophic microbial mats provide an analogue for life in the anoxic Archean. Commun
1021 Earth Environ. 2020;1: 1–10. doi:10.1038/s43247-020-00025-2

1022 25. Lencina AI, Soria MN, Gomez FJ, Gérard E, Farias ME. Composite microbialites: Thrombolite,
1023 dendrolite, and stromatolite associations in a modern environment, Pozo Bravo lake, Salar de
1024 Antofalla, Catamarca Puna, Argentina. J Sediment Res. 2021;91: 1305–1330.
1025 doi:10.2110/jsr.2020.166

1026 26. Vignale FA, Lencina AI, Stepanenko TM, Soria MN, Saona LA, Kurth D, et al. Lithifying and Non-
1027 Lithifying Microbial Ecosystems in the Wetlands and Salt Flats of the Central Andes. Microb
1028 Ecol. 2022;83: 1–17. doi:10.1007/s00248-021-01725-8

1029 27. Farías ME, Villafañe PG, Lencina AI. Integral prospection of Andean microbial ecosystem
1030 project. Microb Ecosyst Cent Andes Extrem Environ biofilms, Microb mats, microbialites
1031 endoevaporites. 2020; 245–260.

1032 28. Nisbet EG, Fowler CMR. Archaean metabolic evolution of microbial mats. Proc R Soc B Biol Sci.

1033 1999;266: 2375–2382. doi:10.1098/rspb.1999.0934

1034 29. Yacobi YZ, Köhler J, Leunert F, Gitelson A. Phycocyanin-specific absorption coefficient:
1035 Eliminating the effect of chlorophylls absorption. Limnol Oceanogr Methods. 2015;13: 157–
1036 168. doi:10.1002/lom3.10015

1037 30. Jørgensen BB, Cohen Y, des Marais DJ, Jorgensen BB, Cohen Y, des Marais DJ. Photosynthetic
1038 action spectra and adaptation to spectral light distribution in a benthic cyanobacterial mat.
1039 Appl Environ Microbiol. 1987;53: 879–886. doi:10.4319/lo.1992.37.8.1813

1040 31. Stomp M, Huisman J, Stal LJ, Matthijs HCP. Colorful niches of phototrophic microorganisms
1041 shaped by vibrations of the water molecule. ISME J. 2007;1: 271–282.
1042 doi:10.1038/ismej.2007.59

1043 32. Miller LC, Martin DS, Liu L-N, Canniffe DP, Miller LC, Canniffe · D P, et al. Composition,
1044 Organisation and Function of Purple Photosynthetic Machinery. Microb Photosynth. 2020;
1045 73–114. doi:10.1007/978-981-15-3110-1_4

1046 33. Blankenship RE, Olson JM, Miller M. Antenna Complexes from Green Photosynthetic Bacteria.
1047 Anoxygenic Photosynthetic Bacteria. Dordrecht: Kluwer Academic Publishers; 1995. pp. 399–
1048 435. doi:10.1007/0-306-47954-0_20

1049 34. Sawicki A, Chen M, Sawicki A, Chen · M. Molecular Mechanism of Photosynthesis Driven by
1050 Red-Shifted Chlorophylls. Microb Photosynth. 2020; 3–42. doi:10.1007/978-981-15-3110-1_1

1051 35. Rosen BP. Biochemistry of arsenic detoxification. FEBS Lett. 2002;529: 86–92.
1052 doi:http://dx.doi.org/10.1016/S0014-5793(02)03186-1

1053 36. Yang HC, Fu HL, Lin YF, Rosen BP. Pathways of Arsenic Uptake and Efflux. Current Topics in
1054 Membranes. Academic Press Inc.; 2012. pp. 325–358. doi:10.1016/B978-0-12-394390-
1055 3.00012-4

1056 37. Willsky GR, Malamy MH. Effect of arsenate on inorganic phosphate transport in Escherichia

coli. J Bacteriol. 1980;144: 366–374. doi:10.1128/jb.144.1.366-374.1980

38. Elias M, Wellner A, Goldin-Azulay K, Chabriere E, Vorholt JA, Erb TJ, et al. The molecular basis of phosphate discrimination in arsenate-rich environments. Nature. 2012;491: 134–137. doi:10.1038/nature11517

39. Saona LA, Soria M, Durán-Toro V, Wörmer L, Milucka J, Castro-Nallar E, et al. Phosphate-Arsenic Interactions in Halophilic Microorganisms of the Microbial Mat from Laguna Tebenquiche: from the Microenvironment to the Genomes. Microb Ecol. 2021;81: 941–953. doi:10.1007/s00248-020-01673-9

40. Ordóñez E, Van Belle K, Roos G, De Galan S, Letek M, Gil JA, et al. Arsenate reductase, mycothiol, and mycoredoxin concert thiol/disulfide exchange. J Biol Chem. 2009;284: 15107–15116. Available: https://pubmed.ncbi.nlm.nih.gov/19286650/

41. Jiang Z, Shen X, Shi B, Cui M, Wang Y, Li P. Arsenic Mobilization and Transformation by Ammonium-Generating Bacteria Isolated from High Arsenic Groundwater in Hetao Plain, China. Int J Environ Res Public Health. 2022;19: 9606. doi:10.3390/ijerph19159606

42. Rascovan N, Maldonado J, Vazquez MP, Eugenia Farías M. Metagenomic study of red biofilms from Diamante Lake reveals ancient arsenic bioenergetics in haloarchaea. ISME J. 2016;10: 299–309. doi:10.1038/ismej.2015.109

43. Ordoñez OF, Lanzarotti E, Kurth D, Cortez N, Farías ME, Turjanski AG. Genome comparison of two Exiguobacterium strains from high altitude andean lakes with different arsenic resistance: identification and 3D modeling of the Acr3 efflux pump. Front Environ Sci. 2015;3. doi:10.3389/fenvs.2015.00050

44. Hoeft McCann S, Boren A, Hernandez-Maldonado J, Stoneburner B, Saltikov C, Stolz J, et al. Arsenite as an Electron Donor for Anoxygenic Photosynthesis: Description of Three Strains of Ectothiorhodospira from Mono Lake, California and Big Soda Lake, Nevada. Life. 2016;7: 1.

1081 doi:10.3390/life7010001

1082 45. Wagner GP, Kin K, Lynch VJ. Measurement of mRNA abundance using RNA-seq data: RPKM
1083 measure is inconsistent among samples. Theory Biosci. 2012;131: 281–285.
1084 doi:10.1007/s12064-012-0162-3

1085 46. Páez-Espino D, Tamames J, De Lorenzo V, Cánovas D. Microbial responses to environmental
1086 arsenic. BioMetals. 2009;22: 117–130. doi:10.1007/s10534-008-9195-y

1087 47. Silver S, Phung LT. Genes and enzymes involved in bacterial oxidation and reduction of
1088 inorganic arsenic. Appl Environ Microbiol. 2005;71: 599–608. doi:10.1128/AEM.71.2.599-
1089 608.2005

1090 48. de Beer D, Meyer V, Klatt J, Li T. Photosynthesis under very high oxygen concentrations in
1091 dense microbial mats and biofilms. bioRxiv. 2018; 335299. doi:10.1101/335299

1092 49. Castillejos Sepúlveda A, Gatti LM, Kerl CF, Chennu A, Klatt JM. Arsenic speciation analysis in
1093 porewater by a novel colorimetric assay. Sci Total Environ. 2022;827: 154155.
1094 doi:10.1016/j.scitotenv.2022.154155

1095 50. Oremland RS, Hoeft SE, Santini JM, Bano N, Hollibaugh RA, Hollibaugh JT. Anaerobic oxidation
1096 of arsenite in Mono Lake water and by a facultative, arsenite-oxidizing chemoautotroph,
1097 strain MLHE-1. Appl Environ Microbiol. 2002;68: 4795–802. doi:10.1128/AEM.68.10.4795

1098 51. Zhang J, Zhou W, Liu B, He J, Shen Q, Zhao FJ. Anaerobic arsenite oxidation by an autotrophic
1099 arsenite-oxidizing bacterium from an arsenic-contaminated paddy soil. Environ Sci Technol.
1100 2015;49: 5956–5964. doi:10.1021/es506097c

1101 52. Franks J, Stolz JF. Flat laminated microbial mat communities. Earth-Science Rev. 2009;96:
1102 163–172. doi:10.1016/J.EARSCIREV.2008.10.004

1103 53. Flores-Kim J, Darwin AJ. The Phage Shock Protein Response. Annu Rev Microbiol. 2016;70: 83–
1104 101. doi:10.1146/ANNUREV-MICRO-102215-095359

1105 54. Junglas B, Huber ST, Heidler T, Schlösser L, Mann D, Hennig R, et al. PspA adopts an ESCRT-III-
1106 like fold and remodels bacterial membranes. Cell. 2021;184: 3674-3688.e18.
1107 doi:10.1016/J.CELL.2021.05.042

1108 55. Sheridan KJ, Duncan EJ, Eaton-Rye JJ, Summerfield TC. The diversity and distribution of D1
1109 proteins in cyanobacteria. Photosynth Res. 2020;145: 111–128. doi:10.1007/s11120-020-
1110 00762-7

1111 56. Lubitz W, Lendzian F, Bittl R. Radicals, radical pairs and triplet states in photosynthesis. Acc
1112 Chem Res. 2002;35: 313–320.
1113 doi:10.1021/AR000084G/ASSET/IMAGES/LARGE/AR000084GF00007.JPEG

1114 57. Budinoff CR, Hollibaugh JT. Arsenite-dependent photoautotrophy by an Ectothiorhodospira-
1115 dominated consortium. ISME J. 2008;2: 340–343. doi:10.1038/ismej.2007.115

1116 58. Blokhina O, Virolainen E, Fagerstedt K V. Antioxidants, oxidative damage and oxygen
1117 deprivation stress: A review. Annals of Botany. 2003. pp. 179–194. doi:10.1093/aob/mcf118

1118 59. Hakala-Yatkin M, Sarvikas P, Paturi P, Mäntysaari M, Mattila H, Tyystjärvi T, et al. Magnetic
1119 field protects plants against high light by slowing down production of singlet oxygen. Physiol
1120 Plant. 2011;142: 26–34. doi:10.1111/j.1399-3054.2011.01453.x

1121 60. Marais A, Sinayskiy I, Petruccione F, Van Grondelle R. A quantum protective mechanism in
1122 photosynthesis. Sci Reports 2015 51. 2015;5: 1–8. doi:10.1038/srep08720

1123 61. Del Razo LM, Quintanilla-Vega B, Brambila-Colombres E, Calderón-Aranda ES, Manno M,
1124 Albores A. Stress proteins induced by arsenic. Toxicol Appl Pharmacol. 2001;177: 132–148.
1125 doi:10.1006/TAAP.2001.9291

1126 62. Latifi A, Ruiz M, Zhang C-C. Oxidative stress in cyanobacteria. FEMS Microbiol Rev. 2009;33:
1127 258–278. doi:10.1111/j.1574-6976.2008.00134.x

1128 63. Jackson CR, Langner HW, Donahoe-Christiansen J, Inskeep WP, McDermott TR. Molecular

1129 analysis of microbial community structure in an arsenite-oxidizing acidic thermal spring.
1130 Environ Microbiol. 2001;3: 532–542. doi:10.1046/j.1462-2920.2001.00221.x

1131 64. Lebrun E, Brugna M, Baymann F, Muller D, Lièvremont D, Lett M-C, et al. Arsenite oxidase, an
1132 ancient bioenergetic enzyme. Mol Biol Evol. 2003;20: 686–93. doi:10.1093/molbev/msg071

1133 65. Grim SL, Dick GJ. Photosynthetic versatility in the genome of Geitlerinema sp. PCC 9228
1134 (Formerly Oscillatoria limnetica 'solar lake'), a model anoxygenic photosynthetic
1135 cyanobacterium. Front Microbiol. 2016;7: 1–14. doi:10.3389/fmicb.2016.01546

1136 66. Sforna MC, Philippot P, Somogyi A, Van Zuilen MA, Medjoubi K, Schoepp-Cothenet B, et al.
1137 Evidence for arsenic metabolism and cycling by microorganisms 2.7 billion years ago. Nat
1138 Geosci. 2014;7: 811–815. doi:10.1038/ngeo2276

1139 67. De Beer D, Schramm A, Santegoeds CM, Kühl M, Kuhl M. A nitrite microsensor for profiling
1140 environmental biofilms. Appl Environ Microbiol. 1997;63: 973–7. Available:
1141 http://www.ncbi.nlm.nih.gov/pubmed/16535560

1142 68. Jeroschewski P, Steuckart C, Kühl M. An Amperometric Microsensor for the Determination of
1143 H 2 S in Aquatic Environments. Anal Chem. 1996;68: 4351–4357. doi:10.1021/ac960091b

1144 69. Klatt JM, Meyer S, Häusler S, Macalady JL, De Beer D, Polerecky L. Structure and function of
1145 natural sulphide-oxidizing microbial mats under dynamic input of light and chemical energy.
1146 ISME J. 2016;10: 921–33. doi:10.1038/ismej.2015.167

1147 70. Revsbech NP. An oxygen microsensor with a guard cathode. Limnology and Oceanography.
1148 John Wiley & Sons, Ltd; 1989. pp. 474–478. doi:10.4319/lo.1989.34.2.0474

1149 71. Tros M, Mascoli V, Shen G, Ho MY, Bersanini L, Gisriel CJ, et al. Breaking the Red Limit:
1150 Efficient Trapping of Long-Wavelength Excitations in Chlorophyll-f-Containing Photosystem I.
1151 Chem. 2021;7: 155–173. doi:10.1016/J.CHEMPR.2020.10.024

1152 72. Cline JD. Spectrophotometric determination of hydrogren sulfide in natural waters. Limnol

Oceanogr. 1969;14: 454–458. doi:10.4319/lo.1969.14.3.0454

73. Bolger AM, Lohse M, Usadel B. Trimmomatic: A flexible trimmer for Illumina sequence data. Bioinformatics. 2014;30: 2114–2120. doi:10.1093/bioinformatics/btu170

74. Li D, Liu C-M, Luo R, Sadakane K, Lam T-W. MEGAHIT: an ultra-fast single-node solution for large and complex metagenomics assembly via succinct de Bruijn graph. Bioinformatics. 2015;31: 1674–1676. doi:10.1093/bioinformatics/btv033

75. Langmead B, Salzberg SL. Fast gapped-read alignment with Bowtie 2. Nat Methods. 2012;9: 357–359. doi:10.1038/nmeth.1923

76. Hyatt D, Chen GL, LoCascio PF, Land ML, Larimer FW, Hauser LJ. Prodigal: Prokaryotic gene recognition and translation initiation site identification. BMC Bioinformatics. 2010;11: 1–11. doi:10.1186/1471-2105-11-119

77. Eren AM, Esen OC, Quince C, Vineis JH, Morrison HG, Sogin ML, et al. Anvi'o: An advanced analysis and visualization platformfor 'omics data. PeerJ. 2015;2015: e1319. doi:10.7717/PEERJ.1319/SUPP-5

78. Aramaki T, Blanc-Mathieu R, Endo H, Ohkubo K, Kanehisa M, Goto S, et al. KofamKOALA: KEGG Ortholog assignment based on profile HMM and adaptive score threshold. Valencia A, editor. Bioinformatics. 2020;36: 2251–2252. doi:10.1093/bioinformatics/btz859

79. Tatusov RL, Galperin MY, Natale DA, Koonin E V. The COG database: a tool for genome-scale analysis of protein functions and evolution. Nucleic Acids Res. 2000;28: 33. doi:10.1093/NAR/28.1.33

80. Buchfink B, Xie C, Huson DH. Fast and sensitive protein alignment using DIAMOND. Nat Methods. 2015;12: 59–60. doi:10.1038/nmeth.3176

81. Blum M, Chang HY, Chuguransky S, Grego T, Kandasaamy S, Mitchell A, et al. The InterPro protein families and domains database: 20 years on. Nucleic Acids Res. 2021;49: D344–D354.

1177 doi:10.1093/nar/gkaa977

1178 82. Jones P, Binns D, Chang HY, Fraser M, Li W, McAnulla C, et al. InterProScan 5: Genome-scale
1179 protein function classification. Bioinformatics. 2014;30: 1236–1240.
1180 doi:10.1093/bioinformatics/btu031

1181 83. Sillitoe I, Dawson N, Lewis TE, Das S, Lees JG, Ashford P, et al. CATH: Expanding the horizons of
1182 structure-based functional annotations for genome sequences. Nucleic Acids Res. 2019;47:
1183 D280–D284. doi:10.1093/nar/gky1097

1184 84. Lu S, Wang J, Chitsaz F, Derbyshire MK, Geer RC, Gonzales NR, et al. CDD/SPARCLE: the
1185 conserved domain database in 2020. - PubMed - NCBI. Nucleic Acids Res. 2020;48: D265–
1186 D268. Available: https://academic.oup.com/nar/article-abstract/48/D1/D265/5645006

1187 85. Pedruzzi I, Rivoire C, Auchincloss AH, Coudert E, Keller G, De Castro E, et al. HAMAP in 2015:
1188 Updates to the protein family classification and annotation system. Nucleic Acids Res.
1189 2015;43: D1064–D1070. doi:10.1093/nar/gku1002

1190 86. Mi H, Muruganujan A, Ebert D, Huang X, Thomas PD. PANTHER version 14: More genomes, a
1191 new PANTHER GO-slim and improvements in enrichment analysis tools. Nucleic Acids Res.
1192 2019;47: D419–D426. doi:10.1093/nar/gky1038

1193 87. Bateman A, Birney E, Durbin R, Eddy SR, Howe KL, Sonnhammer ELL. The Pfam protein
1194 families database. Nucleic Acids Research. 2000. pp. 263–266. doi:10.1093/nar/28.1.263

1195 88. Nikolskaya AN, Arighi CN, Huang H, Barker WC, Wu CH. PIRSF Family Classification System for
1196 Protein Functional and Evolutionary Analysis. Evol Bioinforma. 2006;2: 117693430600200.
1197 doi:10.1177/117693430600200033

1198 89. Attwood TK, Coletta A, Muirhead G, Pavlopoulou A, Philippou PB, Popov I, et al. The PRINTS
1199 database: A fine-grained protein sequence annotation and analysis resource-its status in
1200 2012. Database. 2012;2012. doi:10.1093/database/bas019

1201 90. Sigrist CCJA, Castro E De, … LC-N acids, 2012 undefined, de Castro E, Cerutti L, et al. New and
1202 continuing developments at PROSITE. 2012;41: D344–D347. doi:10.1093/nar/gks1067

1203 91. Letunic I, Bork P. 20 years of the SMART protein domain annotation resource. Nucleic Acids
1204 Res. 2018;46: D493–D496. doi:10.1093/nar/gkx922

1205 92. Brown S, Pegg S, Ojha S, Huang C, Ferrin TE, Babbitt PC. The Structure-Function Linkage
1206 Database. FASEB J. 2006;20. doi:10.1096/fasebj.20.5.a899-c

1207 93. Pandurangan AP, Stahlhacke J, Oates ME, Smithers B, Gough J. The SUPERFAMILY 2.0
1208 database: A significant proteome update and a new webserver. Nucleic Acids Res. 2019;47:
1209 D490–D494. doi:10.1093/nar/gky1130

1210 94. Haft DH, Selengut JD, Richter RA, Harkins D, Basu MK, Beck E. TIGRFAMs and genome
1211 properties in 2013. Nucleic Acids Res. 2013;41. doi:10.1093/nar/gks1234

1212 95. Camacho C, Coulouris G, Avagyan V, Ma N, Papadopoulos J, Bealer K, et al. BLAST+:
1213 Architecture and applications. BMC Bioinformatics. 2009;10: 1–9. doi:10.1186/1471-2105-10-
1214 421/FIGURES/4

1215 96. Kang DD, Li F, Kirton E, Thomas A, Egan R, An H, et al. MetaBAT 2: An adaptive binning
1216 algorithm for robust and efficient genome reconstruction from metagenome assemblies.
1217 PeerJ. 2019;2019: e7359. doi:10.7717/PEERJ.7359/SUPP-3

1218 97. Wu Y-W, Simmons BA, Singer SW. MaxBin 2.0: an automated binning algorithm to recover
1219 genomes from multiple metagenomic datasets. Bioinformatics. 2016;32: 605–607.
1220 doi:10.1093/bioinformatics/btv638

1221 98. Parks DH, Chuvochina M, Waite DW, Rinke C, Skarshewski A, Chaumeil P-A, et al. A
1222 standardized bacterial taxonomy based on genome phylogeny substantially revises the tree of
1223 life. Nat Biotechnol. 2018;36: 996–1004. doi:10.1038/nbt.4229

1224 99. Chaumeil PA, Mussig AJ, Hugenholtz P, Parks DH. GTDB-Tk: a toolkit to classify genomes with

1225 the Genome Taxonomy Database. Bioinformatics. 2020;36: 1925–1927.
1226 doi:10.1093/BIOINFORMATICS/BTZ848

1227 100. Woodcroft BJ, Newell R. wwood/CoverM: Read coverage calculator for metagenomics. Centre
1228 for Microbiome Research, School of Biomedical Sciences, Faculty of Health, Queensland
1229 University of Technology; 2021 [cited 22 Jul 2022]. Available:
1230 https://github.com/wwood/CoverM#readme

1231 101. Wickham H. ggplot2: Elegant Graphics for Data Analysis. Cham: Springer-Verlag New York;
1232 2016. doi:10.1007/978-3-319-24277-4

1233 102. R Core Team. R: A Language and Environment for Statistical Computing. Vienna, Austria; 2020
1234 [cited 3 May 2023]. Available: https://www.r-project.org/

1235 103. Bushnell B. BBMap short-read aligner, and other bioinformatics tools. 2015.

1236 104. Kolde R. CRAN - Package pheatmap. In: https://cran.r-project.org/package=pheatmap
1237 [Internet]. 2019 [cited 12 Jun 2022]. Available: https://cran.r-
1238 project.org/web/packages/pheatmap/index.html

1239

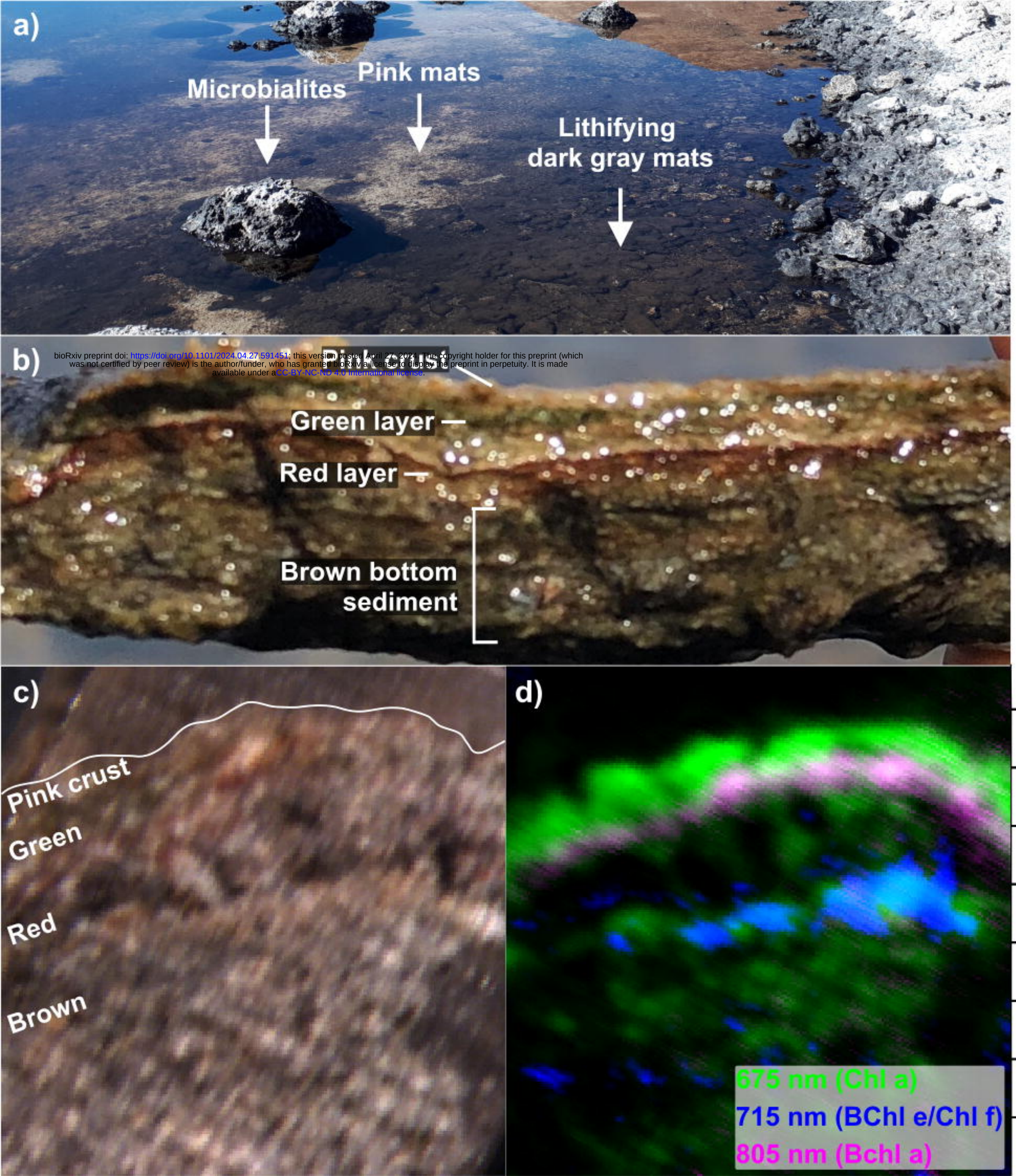

Microbial mat layers

Crust
Green
Red
Brown

0
25
50
75
100

Relative abundance

Class

Alphaproteobacteria
Anaerolineae
Babeliae
Bacilli
Bacteroidia
Bradymonadia
Chitinivibrionia
Chlamydiia
Chloroflexia
Clostridia
Cyanobacteriia
Deinococci
Dojkabacteria
Gammaproteobacteria
Halanaerobiia
Microgenomatia
Phycisphaerae
RBG−13−66−14
Rhodothermia
Spirochaetia
UBA4802
UBA6919
No Class
Unmapped

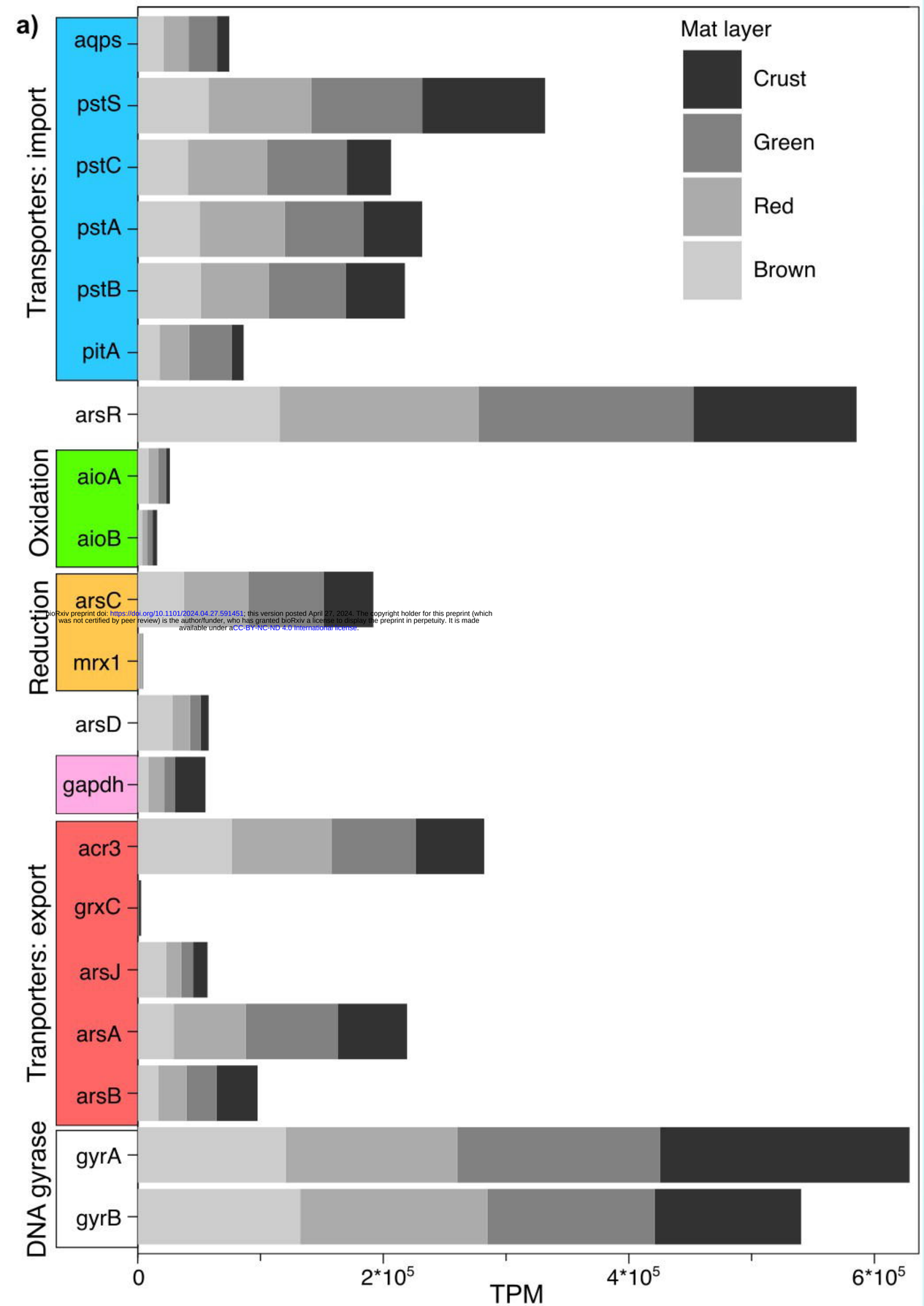

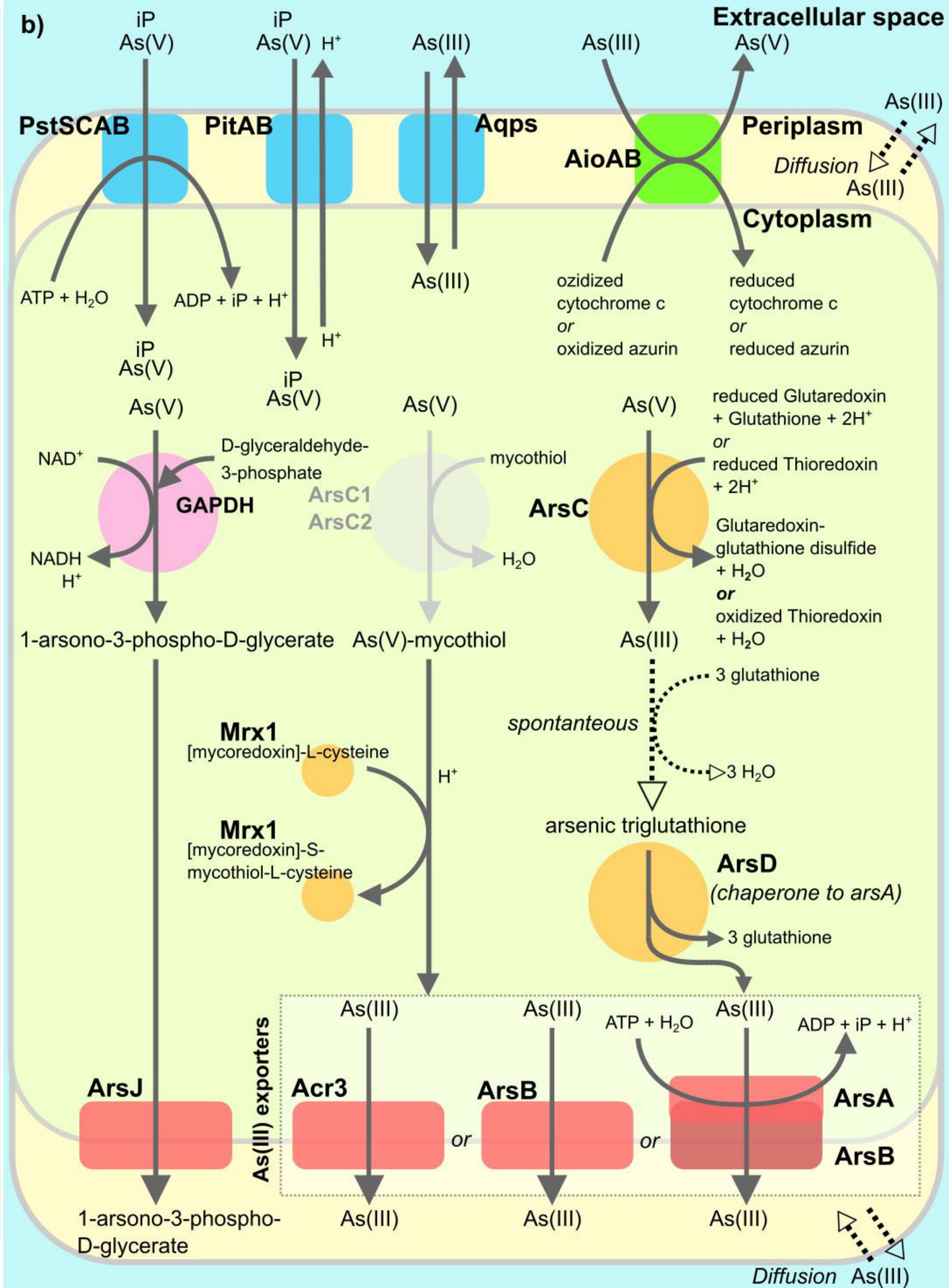

a)

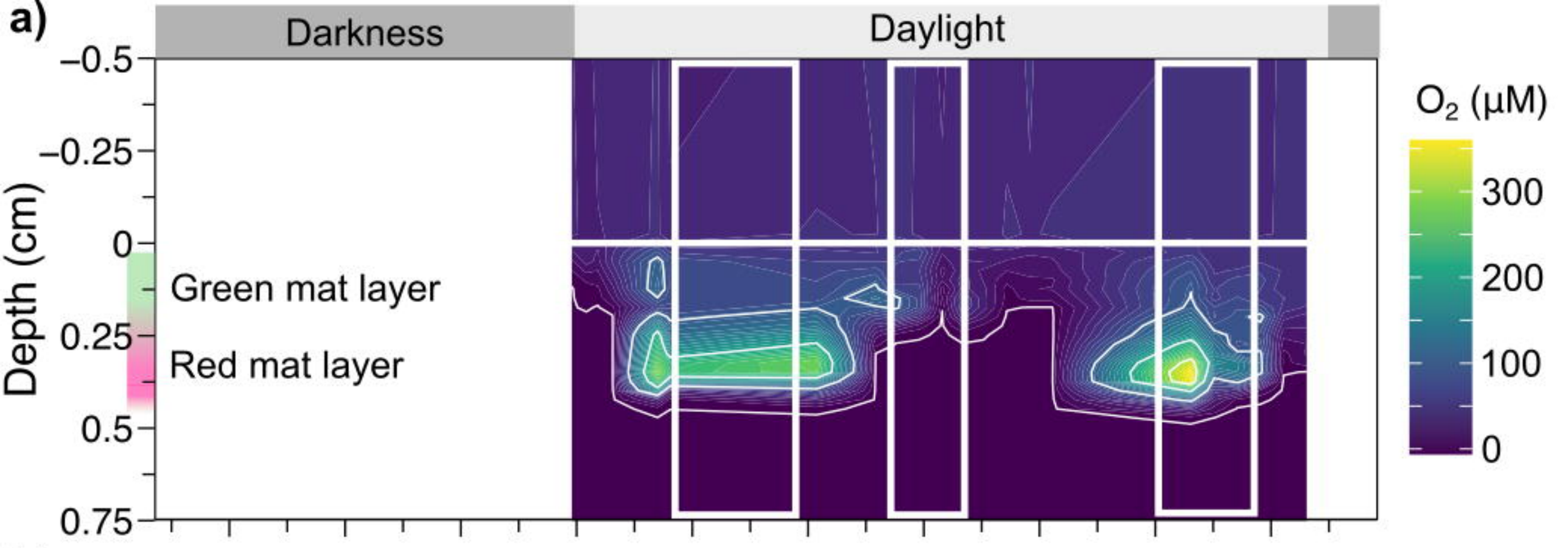

b)

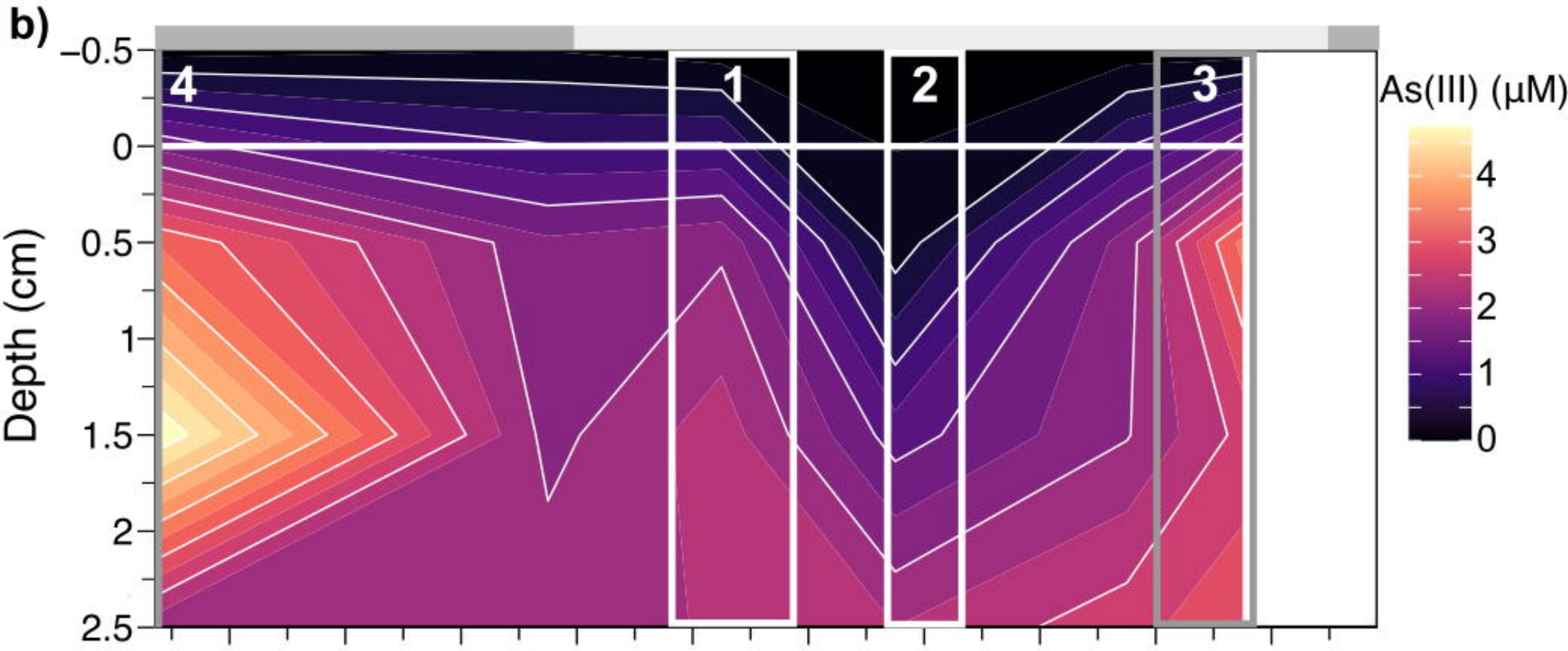

c)

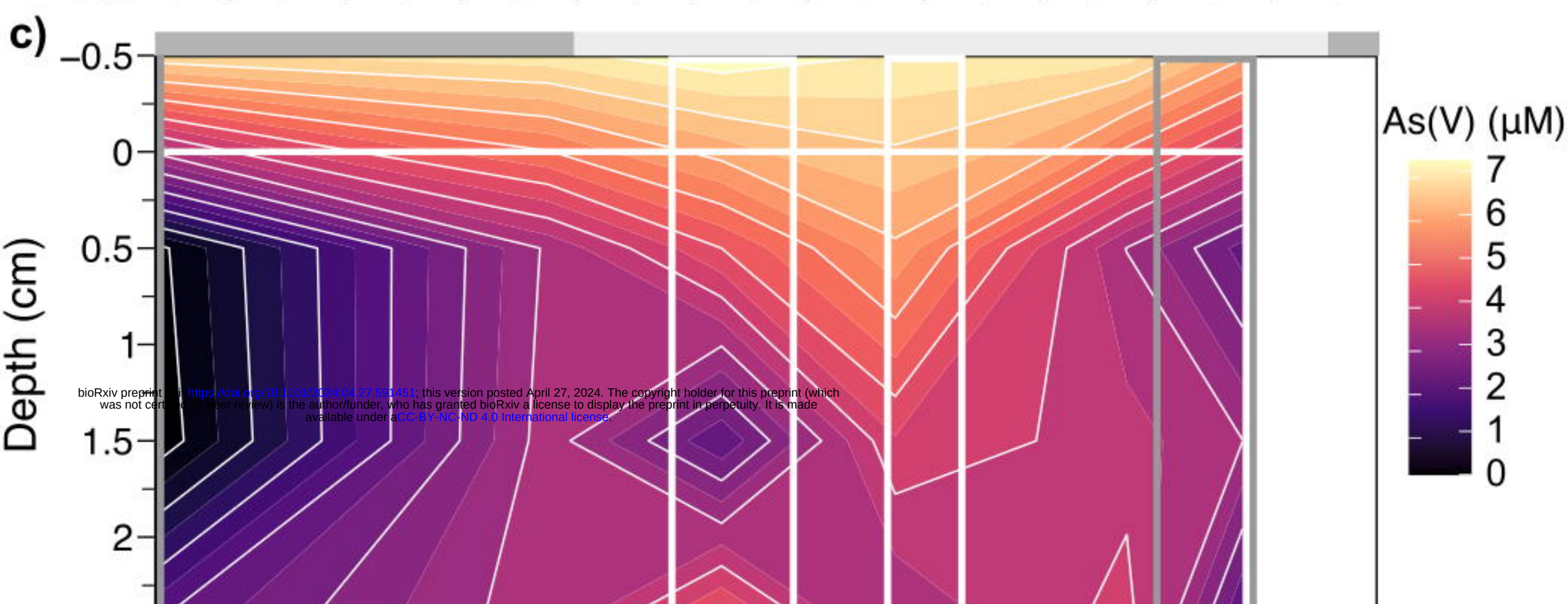

d)

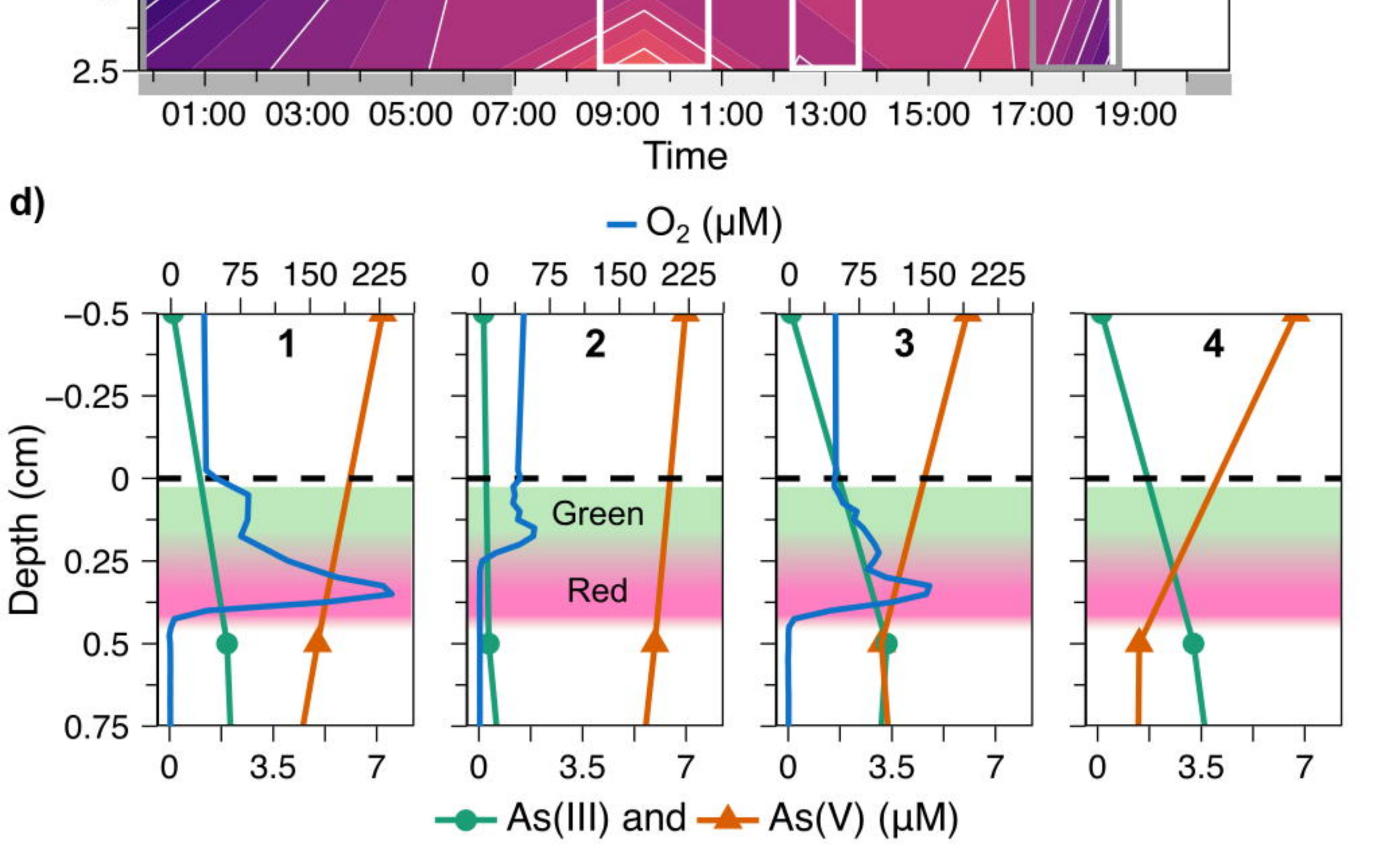

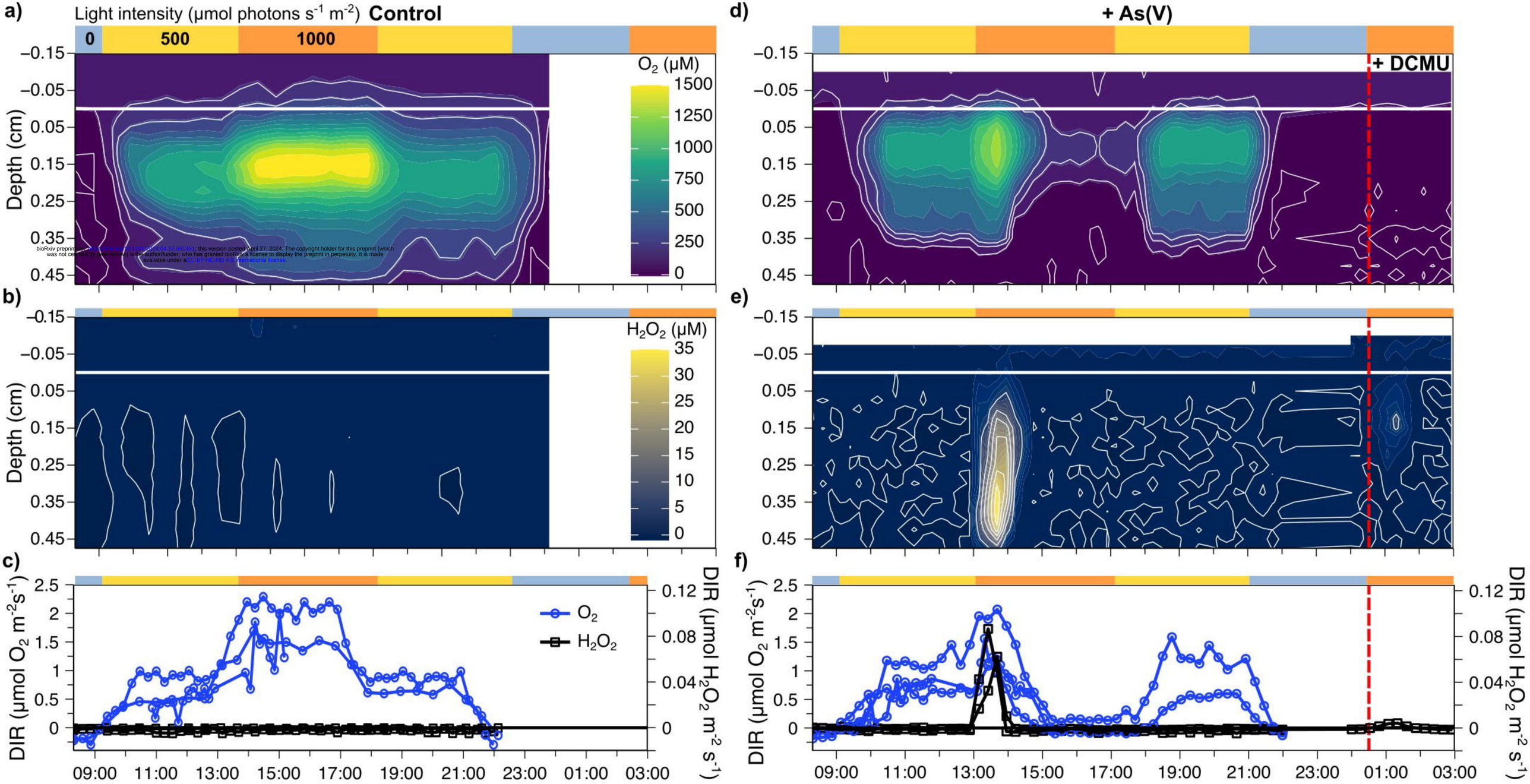

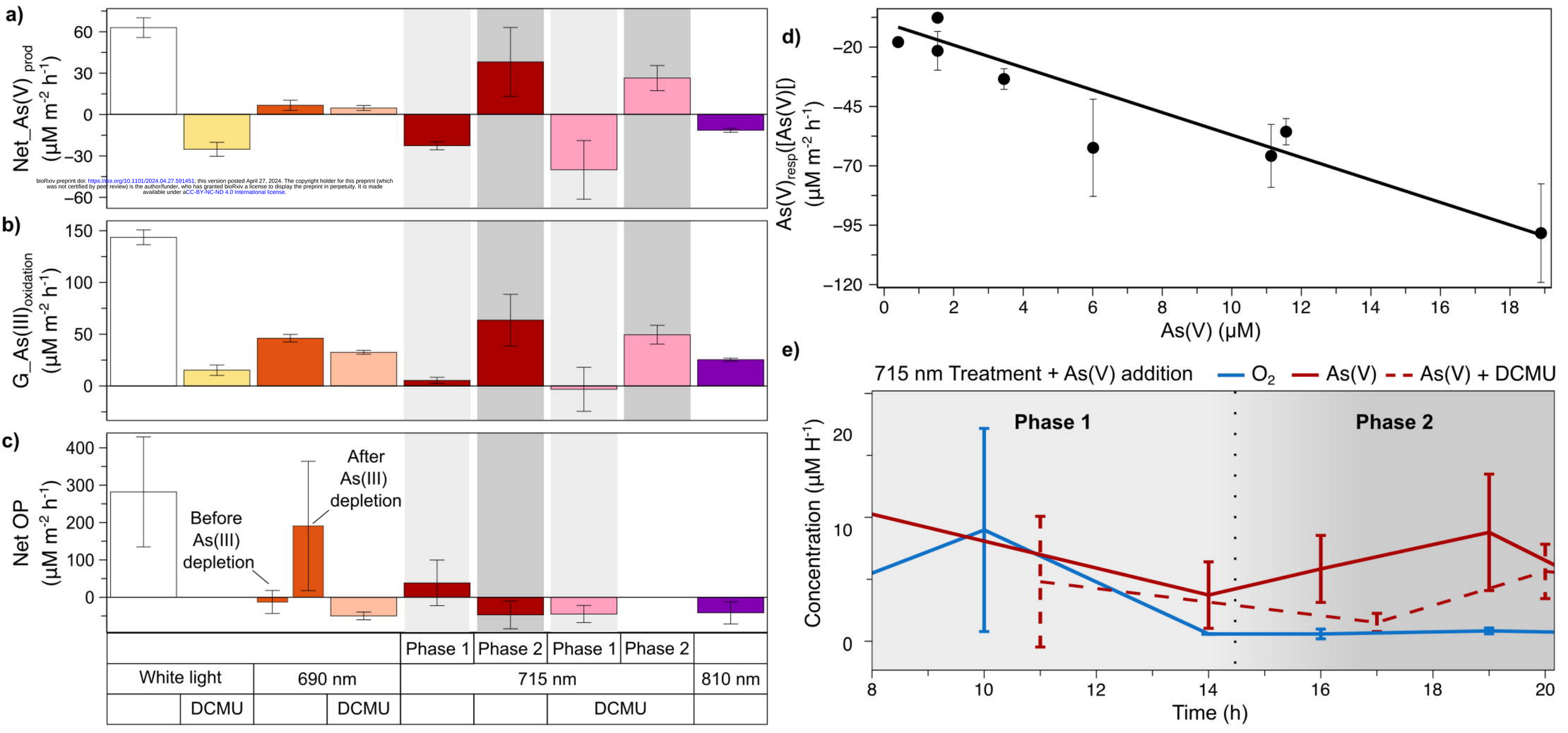

a)

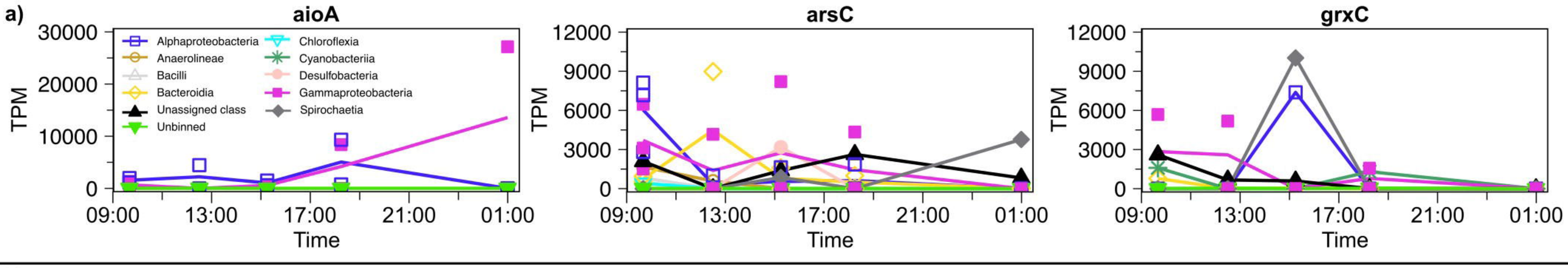

b)